Top Curr Chem (2011) 304: 203–260
DOI: 10.1007/128_2011_153

Published online: 24 May 2011

Integrated Microfluidic Systems for DNA Analysis

Samuel K. Njoroge, Hui-Wen Chen, Małgorzata A. Witek, and Steven A. Soper

Abstract The potential utility of genome-related research in terms of evolving basic discoveries in biology has generated widespread use of DNA diagnostics and DNA forensics and driven the accelerated development of fully integrated microfluidic systems for genome processing. To produce a microsystem with favorable performance characteristics for genetic-based analyses, several key operational elements must be strategically chosen, including device substrate material, temperature control, fluidic control, and reaction product readout. As a matter of definition, a microdevice is a chip that performs a single processing step, for example microchip electrophoresis. Several microdevices can be integrated to a single wafer, or combined on a control board as separate devices to form a microsystem. A microsystem is defined as a chip composed of at least two microdevices. Among the many documented analytical microdevices, those focused on the ability to perform the polymerase chain reaction (PCR) have been reported extensively due to the importance of this processing step in most genetic-based assays. Other microdevices that have been detailed in the literature include those for solid-phase extractions, microchip electrophoresis, and devices composed of DNA microarrays used for interrogating DNA primary structure. Great progress has also been made in the areas of chip fabrication, bonding and sealing to enclose fluidic networks, evaluation of different chip substrate materials, surface chemistries, and the architecture of reaction conduits for basic processing steps such as mixing. Other important elements that have been developed to realize functional systems include miniaturized readout formats comprising optical or electrochemical transduction and interconnect technologies. These discoveries have led to the development of fully autonomous and functional integrated systems for genome processing

S.K. Njoroge, H.-W. Chen, and M.A. Witek
Department of Chemistry, Louisiana State University, Baton Rouge, LA 70803, USA

S.A. Soper (✉)
Department of Chemistry, Louisiana State University, Baton Rouge, LA 70803, USA
and
Department of Mechanical Engineering, Louisiana State University, Baton Rouge, LA 70803, USA
e-mail: chsope@lsu.edu

that can supply "sample in/answer out" capabilities. In this chapter, we focus on microfluidic systems that are composed of two or more microdevices directed toward DNA analyses. Our discussions will primarily be focused on the integration of various processing steps with microcapillary electrophoresis (μCE) or microarrays. The advantages afforded by fully integrated microfluidic systems to enable challenging applications, such as single-copy DNA sequencing, single-cell gene expression analysis, pathogen detection, and forensic DNA analysis in formats that provide high throughput and point-of-analysis capabilities will be discussed as well.

Keywords Continuous flow PCR · DNA analysis · DNA microarrays · Genetic analysis · Integrated microsystems · Microcapillary electrophoresis · Microfluidics · Micro-PCR devices · Solid-phase extraction

Contents

Abbreviations

AOM	Aluminum oxide membranes
BPU	Biochemical processing unit
CAE	Capillary array electrophoresis
CFPCR	Continuous flow polymerase chain reaction
COC	Cyclic olefin copolymer
ddNTPs	Dideoxy nucleoside triphosphates
DNA	Deoxyribonucleic acid
dNTPS	Deoxyribonucleotide triphosphate
DRIE	Deep reactive ion etching
EDTA	Ethylenediaminetetraacetic acid
ELFSE	End-labeled free-solution electrophoresis

EOF	Electroosmotic flow
FPC	Flexible printed circuits
FSCE	Free solution conjugate electrophoresis
HEC	Hydroxyethyl cellulose
HGP	Human genome project
ITO	Indium–tin oxide
LDR	Ligase detection reaction
LPA	Linear polyacrylamides
MDR-TB	Multidrug resistant tuberculosis
MHEC	Methyl hydroxyethyl cellulose
PC	Polycarbonate
PCR	Polymerase chain reaction
PDMS	Poly(dimethylsiloxane)
PEO	Poly(ethylene oxides)
PMMA	Poly(methyl methacrylate)
PPC	Photoactivated polycarbonate
RNA	Ribonucleic acid
RTD	Resistance temperature detector
RT-PCR	Reverse transcription polymerase chain reaction
SGE	Slab gel electrophoresis
SPE	Solid-phase extraction
STRs	Short tandem repeats
TE	Thermoelectric
TTE	*tris*-Taps-EDTA
μCE	Microcapillary electrophoresis
μTAS	Micro-total analysis systems

1 Introduction

1.1 The Human Genome Project

The completion of the human genome sequence in 2003 was one of the most important scientific accomplishments in human history [1] and marked a significant milestone for the human genome project (HGP). This achievement has led to compelling genomic and proteomic research discoveries with unprecedented impacts in areas such as forensic DNA analysis [2–5], medical diagnostics [6, 7], infectious disease management [8–11], and chemical and biological sciences [12, 13]. Some of the important tools for DNA processing include solid-phase extraction (SPE) and purification of DNA, polymerase chain reaction (PCR) or other thermally induced amplification strategies, electrophoresis, and DNA microarrays. Although many conventional benchtop tools currently exist to process DNA samples, efforts are being heavily invested into further automating the processing strategy, reducing the cost of performing the assay, and increasing the sample throughput. In this chapter, we will discuss the use of microfluidics, in particular integrated systems, for processing a variety of DNA samples.

1.2 Molecular Processing Pipeline for DNA Analyses

Complete nucleic acid analyses (RNA or DNA) for a variety of applications can be accomplished using commercial benchtop instruments, and typically consists of several molecular processing steps including:

1. Lysis of cells to release the nucleic acids of interest
2. Purification and isolation of the nucleic acids from other cellular components (e.g., cell debris and proteins)
3. Amplification of trace amounts of nucleic acids to generate sufficient copy numbers for detection
4. Analysis of unique regions within the genetic material using a combination of techniques

To complete an entire assay, a well-equipped laboratory and significant technical expertise are commonly required, with intervention at several stages of the processing pipeline to manipulate samples and/or reagents. In addition, the total time required for sample processing can be several hours to several days.

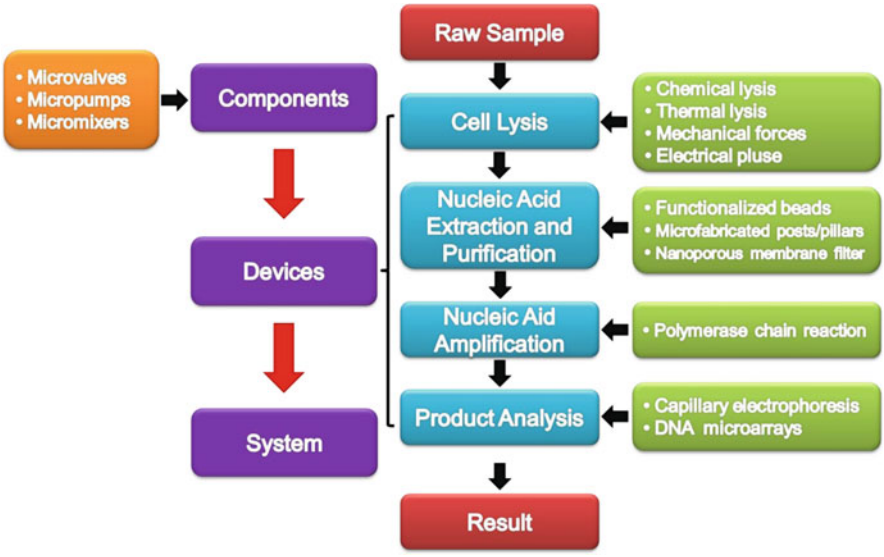

Fig. 1 Flow diagram showing the molecular processing steps required for analyzing nucleic acids. The main steps include cell lysis, nucleic acid extraction and purification, PCR amplification, and analysis methods for identifying the resultant products. For each of the processing steps shown, a device will have poised on it a component for one of these functional steps, and each device may be comprised of various components (such as pumps, valves, and micromixers) in order to carry out the desired operation. A system comprises two or more devices, meaning that it will have integrated onto it multiple processing steps. The ultimate goal is to incorporate all of the molecular processing steps onto a single platform to provide sample in/answer out capabilities with no operator intervention

Derived from the concept of micro-total analysis systems (μTAS) or lab-on-a-chip platforms first proposed by Manz et al. [14] in the early 1990s, integrated microfluidic systems have emerged that incorporate several molecular processing steps into a single platform with sample-to-answer capabilities. These systems are particularly compelling for DNA/RNA analyses. To create such a system, a series of discrete devices performing specific molecular functions such as cell lysis, nucleic acid extraction and purification, nucleic acid amplification, and other supporting analysis techniques (e.g., capillary electrophoresis, microarrays) must be interconnected with minimal dead volumes due to the ultrasmall samples processed (picoliters to nanoliters). Fluids are manipulated using on-chip or off-chip components, such as micropumps, microvalves, and micromixers (see Fig. 1). As noted previously, microsystems are composed of two or more microdevices and, in many cases, microdevices consist of components such as on-chip valves, mixers, and/or pumps. In most cases, DNA/RNA processing requires multiple processing steps and therefore devices need to be combined, either in a single wafer format or a modular format, to form the system targeted for a given genetic analysis (see Fig. 1).

2 Microfluidics and DNA Analysis

The capability of handling a volume of liquid as small as a few nanoliters and even a few picoliters, the common sample size in most microfluidic systems, can be utilized to permit DNA extraction following cell lysis and thermal reactions without creating sample dilution, minimize reagent usage, provide process automation, allow in-the-field analyses, and minimize possible contamination. Microfluidic systems also offer rapid, accurate, and cost-effective analyses. Performing sequencing or genotyping using microfluidic platforms can also lead to significant increases in throughput. For example, DNA sequencing read lengths of 600–800 bases can be achieved in 25 min using microcapillary electrophoresis (μCE) with a separation channel length of 20 cm (Sanger sequencing) [15], whereas the same separation would require 1–2 h in a capillary array electrophoresis (CAE) system [16, 17]. In Sects. 2.1–2.3, we will give a brief introduction to the various microdevices that have been fabricated to handle steps in the processing of nucleic acids, such as cell lysis, extraction and/or purification of the nucleic acids, their amplification, determination of sequence variations, and readout.

2.1 Cell Lysis

Cell lysis is the first step in most DNA analyses and involves disassembly of the cell membranes and release of the genomic material and other cellular contents.

A variety of lysis methods, including chemical lysis [18, 19], thermal lysis [20], and lysis by mechanical forces [21, 22], or electrical pulse [23–26], have been successfully demonstrated in microfluidic devices.

Transitioning the chemical lysis methods commonly used in macroscale work-ups to microfluidic devices is straightforward. Chemical lysis methods involve mixing the target cells with lytic agents, such as sodium dodecyl sulfate or guanidium hydrochloride and hydroxide, that can solubilize the lipid membranes. One issue associated with the use of chemical lysis is that lytic agents can interfere with downstream processing, such as PCR, and therefore must be removed from the sample before subsequent reactions, increasing the microfluidic design complexity. Carol and coworkers [18] reported a polydimethylsiloxane (PDMS) microfluidic device for on-chip cell lysis based on local hydroxide electrogeneration. In this device, hydroxide ions porated the cell membrane, leading to cell lysis. During lysis, hydrogen ions, which were simultaneously generated on-chip, reacted with excess hydroxide ions creating a neutral pH lysate and eliminating the need for a final washing step.

Thermal lysis, which involves disrupting the cell membranes by heating cells to near boiling temperatures, is another method that can be incorporated into a microfluidic device as long as the microfluidic material can withstand the temperature required to lyse the cells. The advantage of thermal lysis is that no interfering reagents are required that may interfere with downstream reactions [27]. The device design can be further simplified by lysing cells in the initial denaturation step of downstream PCRs [28]. But, thermal methods are not applicable for certain cell types, such as Gram-positive bacteria.

Mechanical forces, such as sonication, can be integrated to the microdevice to disrupt cells via gaseous cavitation. In this process, air pockets form from dissolved gases in the aqueous media and collapse rapidly, creating high pressure and high temperature environments sufficient to break cell membranes. This method is suitable for hard-to-lyse cells or spores, but can generate considerable amounts of heat and free radicals [29]. Belgrader et al. [21] reported a minisonicator combined with a spore lysis cartridge. *Bacillus* spores were sonicated in the presence of glass beads and were successfully lysed to release DNA for PCR amplification in ~30 s.

Electrical pulse methods represent another method for cell lysis and are based upon electroporation of the membrane. In the electroporation process, the application of high electric field pulses causes the formation of small pores in cell membranes [30]. However, the use of high electric fields can lead to heating and gas generation. To overcome this limitation, a microfluidic electroporation device for the lysis of human carcinoma cells was demonstrated by Lu et al. [23] In their design, a straight microchannel was constructed in glass, where the side-walls consisted of gold saw-tooth-shaped electrodes supported by the polymer, SU-8. Using pressure-driven flow, cells were directed through the channel and electroporated by the saw-tooth electrodes (see Fig. 2). The magnitude of the electric field was in the range of a few kilovolts per centimeter, while the AC voltage was >10 V peak-to-peak, minimizing heat generation and bubble formation.

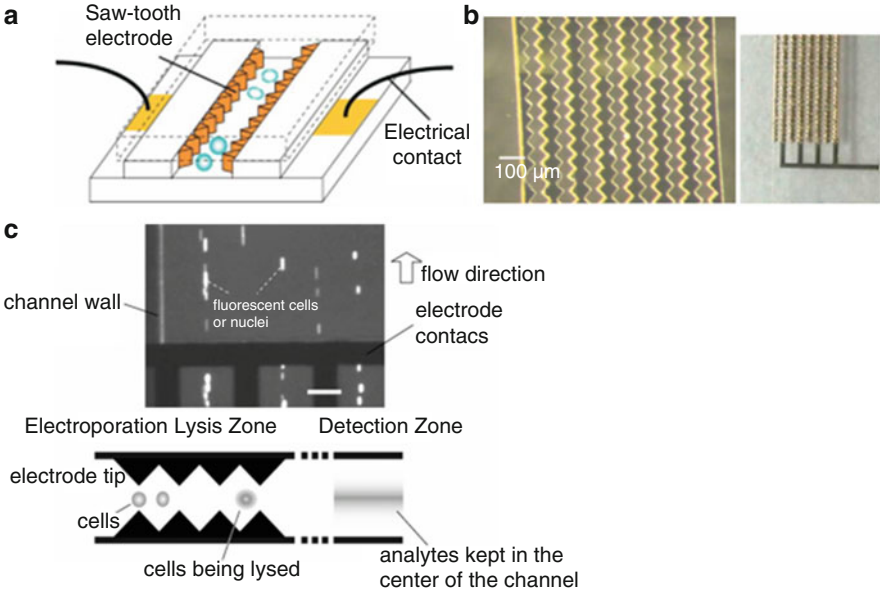

Fig. 2 (**a**) Microelectroporation device for cell lysis. (**b**) Device at various steps of the fabrication process: after metallization and electrode-mold formation (*left*) and after electroplating (*right*). (**c**) Dielectrophoresis (DEP) effect observed in the flow channels (*top*). Saw-tooth microelectrodes acting as a DEP device for focusing intracellular materials after electroporation (*bottom*). Reproduced from [23] with permission

2.2 Nucleic Acid Extraction, Purification, and Preconcentration

Following cell lysis, DNA extraction, purification, and preconcentration are usually achieved by microsolid phase extraction (micro-SPE) devices. This step is essential in order to purify and isolate the genomic materials from other cellular components, contaminants, and chemicals introduced in the cell lysis step that might potentially interfere with downstream enzymatic reactions. In addition, the nucleic acids may be enriched in this phase of the processing strategy to preconcentrate the targets to a level that is amenable for further downstream processing.

A variety of well-established macroscale SPE methods for nucleic acid extraction have been successfully transferred to microscale devices [10, 31–57]. Although the physical principles of these methods may be different (e.g., chaotropic interactions, electrostatic interactions, affinity interactions, etc.), micro-SPE protocols typically consist of three steps: (1) selective adsorption of nucleic acids onto a solid phase; (2) removal of contaminants by a washing step; and (3) elution of the preconcentrated nucleic acids from the solid support using water or a low salt buffer [31]. Like their macroscale counterparts, micro-SPE devices possess a loading level of target material that is dependent upon the available surface area within the extraction bed and, thus, are manufactured either by packing the solid phase

(typically consisting of silica beads) into the device or by directly fabricating microstructures inside the device to increase the available load capacity of the device.

As noted above, micro-SPE devices can be fabricated by packing silica beads, sol–gel immobilized silica beads, photopolymerized monoliths, or modified magnetic particles into microfabricated channels [10, 31–43]. For example, Landers and his research group [32] demonstrated the extraction of PCR-amplifiable DNA from lysed white blood cells using silica particles packed into a capillary tube; the DNA recovery was found to be ~70% in a 10 min processing time. The load of DNA into the device was found to be on the order of 10–30 ng/mg of DNA. To circumvent the high backpressure introduced by flowing silica beads into a microchannel and to improve reproducibility, a silica bead/sol–gel hybrid matrix was packed into a glass microchip (see Fig. 3a) [31, 33]. Other matrices, such as a sol–gel monolith [35] or photopolymerized monoliths [36] were explored by the same group in an effort to overcome the aging and shrinkage problems associated with the silica bead/sol–gel hybrid matrix. Klapperich and coworkers [37–39] used a similar photopolymerized monolith as a solid-support matrix to confine silica beads within a cyclic olefin copolymer (COC) microchip to extract a variety of samples, such as lambda

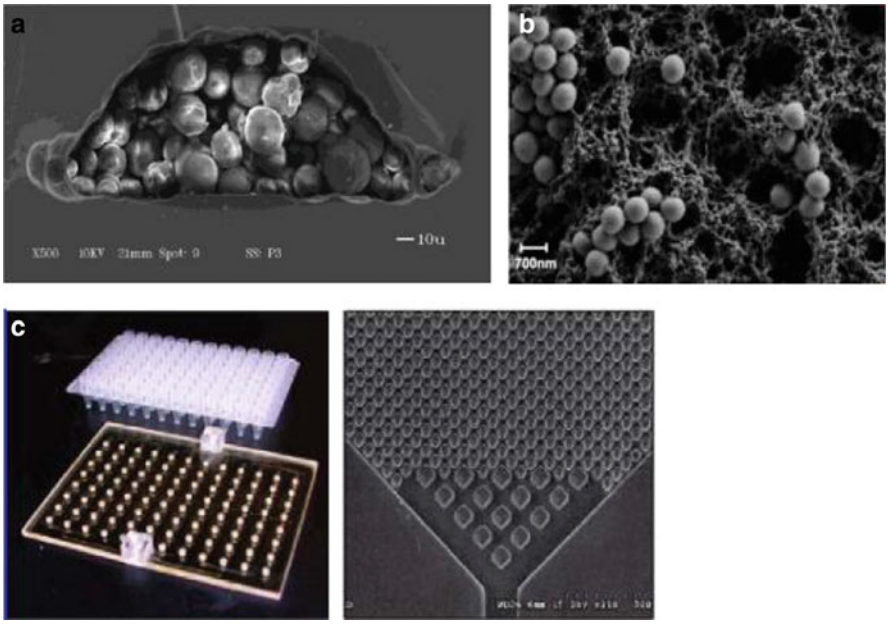

Fig. 3 (**a**) SEM image of the cross-section of a glass microchip channel packed with silica bead/sol–gel hybrid at 500× magnification. Reproduced from [33] with permission. (**b**) SEM image of a porous polymer monolith filled with silica beads at10,000× magnification. Reproduced from [39] with permission. (**c**) Photograph of a 96-well polycarbonate solid phase extraction microfluidic plate and a commercial 96-well titer plate (*left*). SEM image of the micropillars that were fabricated in the purification bed (*right*). Reproduced from [47] with permission

(λ)-DNA, Gram-positive and Gram-negative bacterial genomic DNA, inoculated human blood and urine samples (see Fig. 3b).

Issues associated with SPE beds comprised of silica beads or polymerized polymer monoliths include: (1) residual chaotropic reagents, such as guanidinium or sodium iodide salts, present in the initial elution phase and interfering with downstream amplification steps; (2) packing the matrix, which requires a postfabrication process that can be tedious and demands experienced engineers to accomplish; and (3) aging and shrinkage of the packing material, which can affect the efficiency and reproducibility of the extraction process.

Alternatively, one can produce a SPE surface directly in the device via microfabrication techniques. Micropost or micropillar structures can be fabricated inside the extraction chamber to increase the available surface area, thus enhancing the load of target material as well as the interaction probability between the solution-borne nucleic acids and the SPE bed. Christel et al. [44] fabricated, using deep reactive ion etching (DRIE) and anodic bonding, a micro-SPE device in silicon that contained high aspect ratio (aspect ratio = structure height divided by structure diameter) micropillars with a total surface area of 3.5 mm^2. The binding capacity of DNA was found to be 40 ng/cm^2 with a 50% extraction efficiency for short (500 bp) and medium sized (48 kbp) DNAs. Cady et al. [45] extended this work to *Escherichia coli* cell lysates. To circumvent the tedious DRIE and bonding processes required for fabricating these high aspect ratio microstructures in silicon, Soper and coworkers[46] developed a micro-SPE device made from photoactivated polycarbonate (PPC). This micro-SPE device contained high aspect ratio (5/1) micropillars, hot embossed from a LIGA-fabricated nickel molding tool. The SPE bed possessed a total active surface area of 2.3×10^7 μm^2. Nucleic acids were selectively immobilized onto the PPC surface, which contained carboxylic acid groups generated using UV radiation, using an immobilization buffer containing polyethylene glycol, NaCl, and ethanol. After cleanup using ethanol, the purified and concentrated nucleic acids were eluted from the PPC surface using water or PCR buffer. The load capacity and recovery of *E. coli* genomic DNA were estimated to be 790 ng/cm^2 and 85 ± 5%, respectively. This work was followed by a report on the fabrication of a high-throughput device consisting of 96 micro-SPE beds, each containing an array of 3,800 20-μm diameter micropillars (see Fig. 3c) [47, 48]. Both genomic DNA and total RNA could be extracted and purified from bacterial cells seeded into mammalian blood samples.

Another approach for the SPE of nucleic acids is the use of commercially available nanoporous aluminum oxide membranes (AOM). In a high salt concentration buffer, genomic DNA or RNA will aggregate and bind to the nanoporous membrane; both nanofiltration and electrostatic interactions contribute to the retention and purification of the target DNA or RNA. The retained DNA/RNA can be recovered using a PCR buffer. Kim et al. [49] investigated the extraction of genomic DNA from blood samples with a recovery of ~90% using an AOM sandwiched between PDMS microchannels. The AOM SPE device was later integrated to a microchamber PCR device, demonstrating successful amplification of both DNA from a bacterial sample and RNA from virus samples [50]. The advantages

of this method included the ability to use high flow rates to shorten processing time and low protein absorption onto the AOM. However, the handling of the thin and brittle AOM remains a challenge.

In addition to genomic DNA or RNA purification and preconcentration before an amplification step, some applications, for example the purification of dye terminator Sanger sequencing products, require high quality DNA free of background species such as salts, unincorporated primers, dNTPs, and dye-labeled ddNTPs prior to the electrophoresis step. Soper and coworkers [51] demonstrated the use of a PPC micro-SPE device for the purification of Sanger sequencing products to provide high quality DNA free from background species. PPC micro-SPEs were successfully coupled to capillary gel electrophoresis [54] that also contained a continuous flow Sanger extension thermal cycler [51, 52].

Mathies and his group [53] purified Sanger extension products using a microchamber containing a sparsely crosslinked polyacrylamide gel copolymerized with complementary oligonucleotide probes appended onto the target DNA products. DNA elution was achieved by thermal denaturation of the hybrids. This microchamber was coupled to a Sanger extension chamber and microchip electrophoresis to form an integrated Sanger sequencing bioprocessor. With a 400-fold reduction in sequencing reagents and 10- to 100-fold reduction in DNA template required compared to benchtop approaches, 556 continuous bases were sequenced using this bioprocessor with 99% accuracy [54].

2.3 Microfluidic Polymerase Chain Reactors

Since the discovery of the PCR in 1986 by Mullis et al., [58] PCR has become a crucial tool in basic molecular biology discovery, genome sequencing, clinical research, in vitro diagnostics, and evolutionary studies [59]. PCR is an enzymatic reaction that allows any nucleic acid fragment to be generated in vitro and in high abundance. Theoretically, the amount of product doubles during each PCR cycle, as shown by the following equation:

$$N = N_0 2^n, \tag{1}$$

where N is the number of amplified DNA molecules, N_0 is the initial copy number of DNA molecules and n is the number of amplification cycles [60, 61]. Experimentally, the amplification efficiency (E) can range from 0 to 1, and therefore the true copy number produced is given by:

$$N = N_0 (1 + E)^n. \tag{2}$$

In PCR, denaturation and annealing are nearly instantaneous events that occur as soon as the correct temperature is reached (e.g., ~94 °C for denaturation; 50–60 °C

for annealing) and the extension step is limited only by the kinetics of the polymerase enzyme. Implementation of the thermostable *Taq* polymerase as a substitute for the Klenow fragment of *E. coli* DNA polymerase I [62] has made it possible to automate the PCR amplification step by using various thermal cycles carried out by a block thermal cycler. Investigators have shown that *Taq* DNA polymerase has an extension rate of 60–100 nucleotides/s at 72 °C [63]. For efficient amplification, a device with low heat capacity that can transfer heat quickly to the sample and quickly draw away the heat when cooling is preferable. Most conventional thermal cyclers have large thermal masses resulting in high power requirements and slow heating and cooling rates with long reaction times, typically exceeding 1.5 h in spite of the fact that kinetically, a 500 bp PCR product should be produced in as little as 5 s.

Due to the intrinsically small PCR chamber volumes and mass, exquisite heat transfer capabilities can be realized in microfluidic polymerase chain reactors (micro-PCR) devices that can significantly reduce the processing time compared to conventional benchtop thermal cyclers. Short thermal cycling times can be realized and still provide amplification efficiencies comparable to their macroscale counterparts with designs that are sometimes not conducive to macroscale formats. Micro-PCR devices have adopted design formats such as chamber-type PCR devices, in which the PCR cocktail and target are mixed inside a microchamber and the chamber is then cycled between the various temperatures required for the amplification process. Another design approach uses the continuous-flow format, in which the PCR device consists of isothermal zones brought to equilibrium prior to the amplification process. The PCR cocktail is shuttled between these isothermal zones either electrokinetically or hydrodynamically to affect the thermal processing. Another format that has been employed for microscale PCR devices is a thermal convection-driven PCR device in which a temperature gradient is applied to a closed reaction chamber and the fluid is shuttled through the temperature gradient using a Rayleigh–Bénard convection cell. In Sects. 2.3.1–2.3.4, we will briefly introduce these PCR designs.

2.3.1 Chamber-Type Micro-PCR Devices

In chamber-type micro-PCR devices, a static PCR cocktail containing the target is repeatedly cycled between three different temperatures: one for denaturation, a second for renaturation, and a third for polymerase extension, which is similar to that used in a conventional PCR thermal cycler. Chamber-type micro-PCR devices consist of either a single chamber or multiple chambers configured on a single wafer with the appropriate heating modalities to allow thermal cycling. The primary advantage of these types of microthermal cyclers is the low thermal masses that must be heated/cooled, providing faster reaction times compared to block thermal cyclers.

2.3.2 Single-Chamber Micro-PCR Devices

In 1993, Northrup et al. [64] reported the first PCR microfluidic device, which consisted of a 50-μL well structure serving as the reaction chamber and was fabricated in silicon using wet chemical etching. Twenty amplification cycles were carried out, with the cycling time four times faster than a conventional benchtop PCR device. In 1994, Wilding et al. [65, 66] developed a silicon/glass hybrid device that held 5–10 μL of reaction mixture in a chamber, whose performance was improved by surface passivation through salinization of the microchamber surface[67] and which was heated using an external copper block. Single-chamber PCR devices have been widely investigated since these initial reports [68–77]. However, single-chamber micro-PCR devices possess low throughput.

2.3.3 Multichamber Micro-PCR Devices

Multiple PCR chambers have been fabricated on a single microfluidic chip and explored for high throughput PCRs [78–83]. An example of a multichamber micro-PCR device, the micro-DNA amplification and analysis device, (μ-DAAD) consisted of 16μ-DAADs in parallel with each μ-DAAD consisting of four microreactors fabricated on a 4″ silicon wafer (see Fig. 4). Multichamber micro-PCR devices [84] have been demonstrated for DNA amplifications of five gene sequences related to *E. coli* from three different DNA templates and detected by TaqMan chemistry with a limit of detection (LOD) of 0.4 copies of target DNA.

2.3.4 Continuous Flow PCR Devices

Another configuration for micro-PCR devices employs a flow-through format with a "time–space conversion" concept, in which the sample is continuously transitioned through isothermal zones for denaturation, annealing, and extension. This is in contrast to chamber-type PCR devices, in which heating and cooling occurs on a static sample with the entire device heated and cooled to the desired temperatures [79, 83, 85, 86]. The continuous flow PCR (CFPCR) approach allows for short reaction times because the small-volume fluid elements can be heated or cooled to the required temperature within 100 ms [59]. In 1998, Kopp et al. [87] reported the first CFPCR microdevice (see Fig. 5). This device consisted of 20 thermal cycles comprised of a serpentine channel design whose dimensions were 40 μm in width and 90 μm in depth, with a total length of 2.2 m, producing a pressure drop of ~14.5 PSI. For DNA amplification, 10 μL of a PCR mixture was hydrostatically pumped at volumetric flow rates ranging from 5.8 to 72.9 nL/s with a flow-through time of 18.7–1.5 min [87]. The channel walls were silanized with dichlorodimethylsilane to reduce possible adsorption of the polymerase enzyme (*Taq* polymerase) and DNA

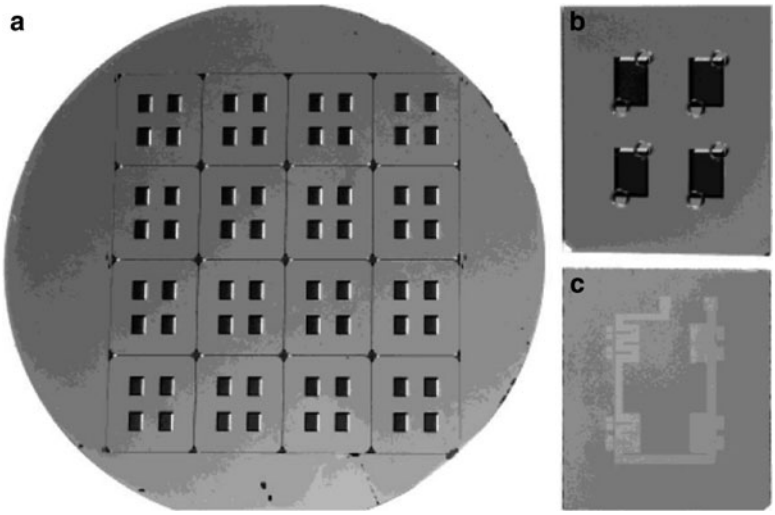

Fig. 4 Photographs of μ-DAAD production steps. (**a**) Front side of a 4″ silicon wafer populated with etched microreactors; 16 μ-DAAD are processed in parallel, each consisting of four microreactors. (**b**) Front-side view of a single μ-DAAD (16 × 1 mm^2) after bonding a cover plate and dicing. DNA arrays are printed onto the bottom of the microreactor cavities, but cannot be seen in this image because of their small size. Holes of 1 mm in diameter are drilled in the cover glass for the filling of the μ-DAAD reactors with reagent. (**c**) Back-side view of the device with platinum heater coil and thermoresistors placed at the corresponding area of the microreactor. Reproduced from [79] with permission

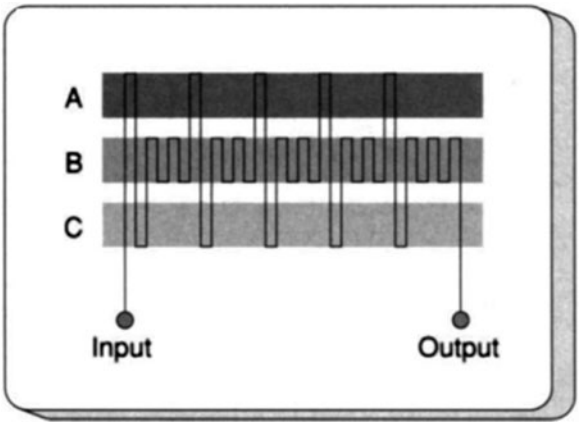

Fig. 5 Chip for CFPCR. Three well-defined isothermal zones are poised at 95 °C (*A*), 77 °C (*B*), and 60 °C (*C*) by means of thermostated copper blocks. The sample is hydrostatically pumped through a single channel etched into a glass wafer. The channel passing through the three temperature zones defines the thermal cycling process. Reproduced from [87] with permission

onto the glass surface. A zwitterionic buffer and nonionic surfactant were used as the PCR buffer additives to impart a dynamic coating [88].

Using a 20-cycle spiral microchannel hot embossed into a polycarbonate (PC) substrate configured for performing CFPCR [89], the PCR cycle time was reduced

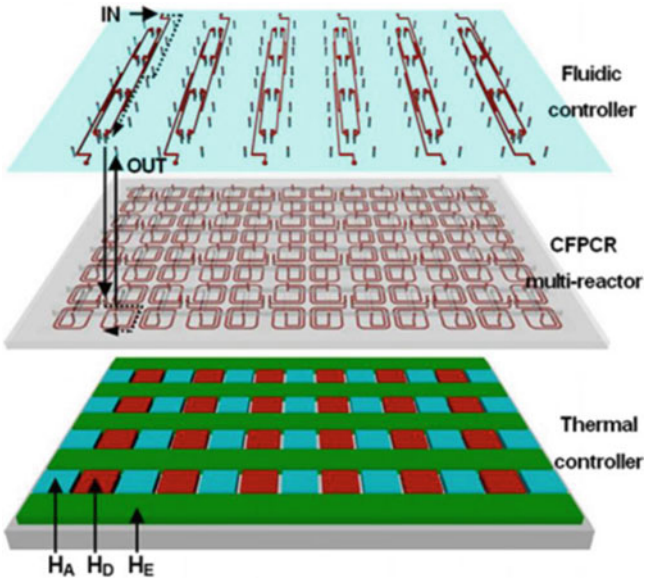

Fig. 6 High-throughput CFPCR multireactor platform consisting of three functional units: a fluidic controller for distributing reagents and analyte to the reactors, a CFPCR multireactor, and a distributed temperature controller. H_D denotes the denaturation heaters (90–95 °C), H_A annealing heaters (50–70 °C), and H_E extension heaters (70–77 °C). Reproduced from [92] with permission

to the kinetic limit set by the polymerase incorporation rate; 500- and 997-bp fragments were amplified in a total time of 1.7 min (5.2 s/cycle) and 3.2 min (9.7 s/cycle), respectively. The amplification efficiency was further optimized through proper thermal management using numerical models and experiments to evaluate the effects of different combinations of temperature distribution in a typical CFPCR device fabricated by hot embossing PC substrates [90]. Chen et al. [91–93] reduced the footprint of each spiral reactor to 8 mm by 8 mm and arranged 96 reactors in titer-plate format (12 × 8) for high throughput processing (Fig. 6).

The attractive features of CFPCR devices consist of: (1) very rapid heat transfer during the PCR, with run times on the order of minutes; (2) low possibility of contamination (closed architecture); [4, 10, 94] and (3) facile integration with various liquid transport processes, such as magneto-hydrodynamic (MHD) actuation [95]. Additional advantages include reduced sample consumption and reagents (lower cost) and simple integration to other DNA processing devices [11, 96]. A limitation of this approach is the fixed cycle number that can be employed by the chip, which is dictated by the device layout. To overcome this drawback, Chen et al. [97] demonstrated the use of a microfabricated PC chip for DNA amplification in a continuous flow (CF) mode using electrokinetically driven synchronized pumping (Fig. 7). A 500-bp fragment from λ-DNA was obtained with a total time of amplification of ~18.1 min for 27 cycles.

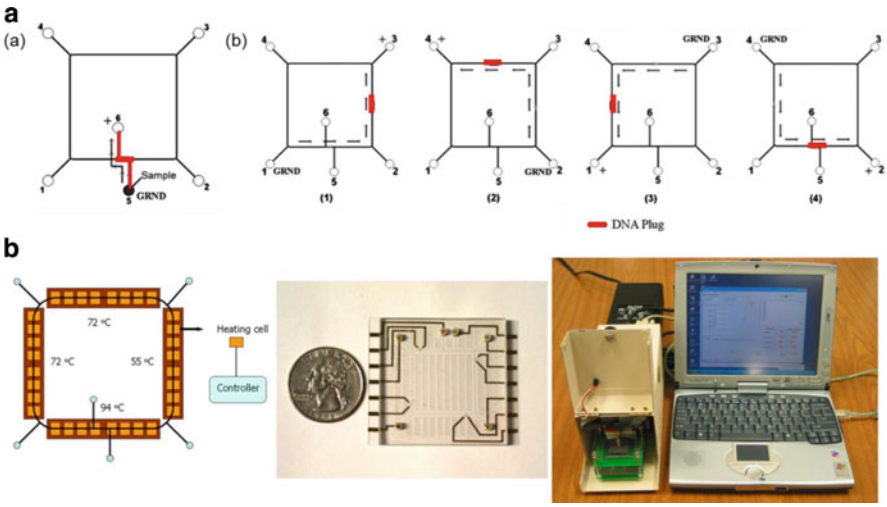

Fig. 7 (**a**) Principle of electrokinetic synchronized cyclic CFPCR process. Sample injection (*a*): DNA was filled into reservoir *5* and a voltage was applied to the electrodes in reservoirs *5* (*GRND* indicates ground) and *6* (+ indicates high voltage input). Sample moved across the reactor channel to fill the crossed-T injector. Sample cycling (*b*): Following injection, the sample is shuttled through the various isothermal zones by moving the position of the applied electric field in a cyclic fashion as denoted in diagrams *1–4*. (**b**) Schematic view and photographs of the electrokinetically synchronized CFPCR microchip. The actual microchip, fabricated via replication technology into PC, is shown in the *middle photograph* next to the quarter. Poised on the PC chip are electrode contacts for applying the voltaged in an automated fashion to the various reservoirs. Reproduced from [97] with permission

The arrangement of the three temperature zones on most rectangular serpentine channel CFPCR devices consists of denaturation, extension, and annealing in that order. Although this arrangement can establish a smooth temperature gradient, amplification efficiency may degrade because the melted single-stranded DNA (ssDNA) is likely to form double strands with the template DNA or with their complementary fragments when passing through the extension zone. To circumvent this problem, a novel three temperature zone arrangement in a "circular" format consisting of denaturation, annealing, and extension has been exploited [95, 98–100].

The PCR channel for these CFPCR devices can also consist of either capillary tubes [99, 100] or an on-chip annular channel [95, 101]. The serpentine channel formats on a monolithic chip can utilize thermal insulation with the aid of air gaps [102, 103] or by utilizing glass chips with a low thermal conductivity [104, 105]. Recently, a novel spiral channel configuration was also used to perform CFPCR on a single PC wafer with a circular arrangement of three temperature zones, allowing for a compact footprint and a minimal number of heaters for temperature control [106, 107]. CFPCR microfluidics can also use a unidirectional PCR or oscillatory flow [108].

2.4 *Microfluidic Thermal Heating Methods*

The choice of a heating method for micro-PCR devices is important in achieving efficient temperature ramping rates. The diversity of materials exhibiting differences in thermal mass means that different heating methods may be required. At present, temperature cycling on microfluidic devices can be performed either with contact or noncontact heating methods. Summarized below are various heating methods that have been employed in microfluidic devices.

2.4.1 Contact Heating

For contact heating, heaters are fabricated directly within the microchip or are in contact with the outside of the microchip. Contact heating utilizes an electrothermal conversion to heat the PCR solution [109]. Contact heating can be achieved through the use of thin film heating elements, which are mainly fabricated using deposition techniques; through the use of metal heating blocks, which primarily consist of inserting a heating cartridge into the metal blocks; or by utilizing Peltier elements.

2.4.2 Thin Film Heating

Heating elements can be fabricated on-chip using thin film deposition. Platinum [78, 79, 110–114] is the most commonly used material for heating elements due to its ability to withstand high temperatures, good chemical stability, and ease of micromanufacturing. Some other metals, alloys, or inorganic compounds have also been used as thin film heaters in micro-PCR devices, such as Al [70, 81, 82, 115], Ni [104], W [101], Ag/graphite inks [85], Ag/Pd [102, 116], Ni/Cr [117], Cr/Al [82], Al_2N_3 [118], and indium–tin oxide (ITO) [119–121]. Microheaters fabricated by Pt thin film deposition often require a thin layer of Ti serving as an adhesion layer. The Ti layer exhibits a high diffusion rate at high temperatures, which can deteriorate the Pt heater [122]. Commercial thin film resistive heaters [85, 106, 107] have proven to be efficient and robust for achieving fast PCR cycling, in contrast to conventional PCR devices.

2.4.3 Metal Heating Blocks

Conventional PCR instruments typically utilize contact heating, which involves a metal heating block in contact with the sample container, to cycle the temperature of the PCR solution that is held within a thin-walled polypropylene tube. In spite of their large thermal mass and slow temperature ramping rates, metallic heating blocks and Peltier-based thermo-electric (TE) ceramic heating blocks are widely applied in micro-PCR devices [69, 84, 87, 123–128]. To achieve fast thermal transition, two [8, 98, 123, 129] or more TE devices can be coupled to thermally cycle the PCR solution, and a total of six TE devices have been used in a portable

miniaturized thermal cycling system [84]. The temperature of the peltiers could be independently controlled and programmed to be at different temperature levels necessary for effective annealing and denaturation. To ensure good thermal contact between the TE element and the cycled region of the device, supporting substances with higher thermal conductivity, such as mineral oil [8, 129] or a metallic thin wafer [130], can be added to the interface of the TE element. Normally, the TE cell consists of an array of parallel P–N junctions and each parallel P–N junction establishes its own temperature differential for a given voltage. The P–N junction is formed by joining P-type and N-type semiconductors (e.g. silicon) and Peltier-based TE use the differing behavior of charge carriers in P and N type semiconductor to move heat. Consequently, a radial temperature gradient on the hot surface of the TE cell is created, which causes nonhomogeneity of the surface temperature of the TE cell and compromises the efficiency of the PCR [109]. To achieve a homogenous temperature distribution across the surface of the TE cell, an oxygen-free thin copper wafer is necessary to redistribute the surface temperature [126]. Other reliable contact heaters are resistive heating coils [99, 127, 131] and single-sided flexible printed circuits (FPCs) [132].

It is important to note that the thermal-cycling rate is limited by the thermal mass of the heating element itself and of the entire micro-PCR device as well. Moreover, in the case of an external contact element, localized heating is ultimately limited in terms of lateral resolution by the thermal conductivity of the substrate material. In the case of on-chip integrated heaters, these devices still require tedious and complicated micromanufacturing processes, which restrict the flexibility to reconfigure the PCR design [133].

2.4.4 Noncontact Heating

The inherent problem with contact thermal heaters is their relatively large thermal mass. More thermal mass is added to the PCR device when contacting the chamber containing the PCR solution, which hinders fast thermal cycling rates. For the integration of PCR with μCE, thermal management becomes difficult because contact resource is regarded as part of the PCR chip and not part of the electrophoresis chip itself. These restrictions have triggered interest in the development of noncontact thermal cycling in which the heating is remote from the microfluidic device and not in physical contact with the PCR chamber [109].

2.4.5 Noncontact Heating Based on IR Radiation

Noncontact heating using IR radiation was first reported by Oda et al. [134] in 1998. In their work, an IR light, which used a single and inexpensive tungsten lamp as the noncontact heat source, was used for heating glass microchambers. The authors achieved temperature ramping rates of 10 °C/s for heating and 20 °C/s for cooling. In 2000, Hühmer and Landers [71] reported IR-mediated fused-silica capillary cycling with nanoliter volumes (160 nL), with improved heating and cooling

rates of 65 and 20 °C/s, respectively. Giordano et al. [74] developed a novel polyimide (PI) PCR microchip, which utilized IR-mediated thermal cycling for the amplification of a 500-bp λ-phage DNA fragment in a 1.7-μL chamber with a total reaction time of only 240 s for 15 cycles. In 2003, Ferrance et al. [72] presented IR-mediated PCR amplification of genomic DNA using primers defining a 380-bp fragment of the β-globin gene followed by electrophoretic analysis on a single glass chip for the analysis of Duchenne muscular dystrophy (DMD) in less than 15 min for 35 cycles.

2.4.6 Noncontact Heating Based on Hot Air Cycling

Wittwer et al. [135, 136] developed noncontact heating for PCR based on hot air cycling. In their work, temperature cycling was performed without physical contact between the heating source and the reaction chamber by rapidly switching streams of air set to the desired temperature. Due to the low thermal mass of air, a high temperature ramping rate could be obtained, which has been further improved by several research groups [68, 112, 113, 137–139].

2.4.7 Noncontact Heating Based on Laser-Mediated Heating

The tungsten lamp is a noncoherent source with large focus projection, which limits the heating efficiency when applied to microchips with a small cross-section. Laser-mediated noncontact heating utilizes a photothermal effect produced by a diode laser coherent light source to heat an absorbing target. Tanaka et al. [140] used a diode laser to control the temperature of a chemical reaction by heating an absorbing target of a black ink point placed on top of a glass microchip cover plate above the reaction channel. The integrated glass microchip with noncontact IR laser-mediated heating has been demonstrated for fast and localized temperature control under flowing conditions with ultrafast heating and cooling rates of 67 and 53 °C/s, which is 30 times faster than a conventional device and 3–6 times faster than electrothermal miniaturized thermal cyclers [133]. This heating method may be very attractive and desirable due to its high resolution for spatially localized heating, ease of manipulation along the chip, and its property of being a point light source. Unfortunately, this heating method has not been applied for temperature control in microfluidics.

2.4.8 Noncontact Heating Based on Microwave Irradiation

Noncontact heating utilizing a focused microwave source was demonstrated by Fermér et al. [141]. In their work, a single-mode microwave cavity was used to heat 100 μL of PCR mixture in a 0.5-mL polypropylene tube for 25 cycles. Most recently, microwave-induced milliliter-scale PCR (see Fig. 8) was reported [142] for real-time PCR analysis. Although the amount of amplified nucleic acid product

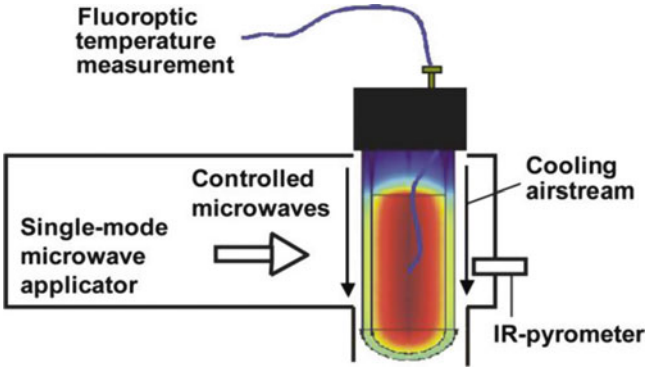

Fig. 8 Experimental set up for microwave-heated PCR that is used to perform milliliter-scale PCR utilizing highly controlled microwave thermal cycling. Reproduced from [142] with permission

after 33 cycles indicated incomplete amplification, which was attributed to temperature "over-shooting" at the denaturation phase and subsequent deactivation of the *Taq* polymerase [143], microwave heating was quite promising due to the following properties [141]:

1. Efficiency of the optimized microwave conditions nearly reached 70% that of conventional PCR
2. Irradiation energy was used to heat only the PCR solution and not a heating block or the sample containment tube
3. Temperature ramping time was substantially shortened
4. Required temperature was reached almost instantaneously and simultaneously, allowing for shortening of the incubation time
5. Modern microwave cavities can deliver a uniform field density without "hot-spots"

2.4.9 Other Noncontact Heating Methods

Other noncontact heating methods have also been described, such as noncontact heating using a halogen lamp as a low power radiation source for rapid temperature ramping in a silicon microreaction chamber [144]. This method achieved a rate of 4 °C/s for heating and 4 °C/s for cooling. Another noncontact heating method is based on induction heating and was first reported by Pal et al. [145]. Induction heaters are much simpler to fabricate, and heating and cooling rates of 6.5 and 4.2 °C/s can be achieved by optimizing the heater dimensions and frequency. The advantage of this method is that accurate positioning of the reaction mixture with respect to the heater is not necessary, deposition steps to pattern thin-film heaters on the chip are not required, and elaborate percentage/integrator/differentiator (PID) control is not needed [144].

Convectively driven PCR is an alternative thermal cycling process, which was first reported in 2002 by Krishnan et al. [146]. The authors used a Rayleigh–Bénard convection cell consisting of a 35-μL cylindrical cavity to perform the PCR amplification of the β-actin gene (295-bp fragment). Rayleigh–Bénard convection is generated by buoyancy-driven instability in a confined fluid layer heated from below [147]. The inherent structure of Rayleigh–Bénard convection-steady circulatory flow between surfaces employs two fixed temperature zones to facilitate the convection-driven sample flow. In contrast to CFPCR, the temperature cycling is achieved as the fluid continuously shuttles vertically between the two temperature zones poised for annealing/extension (top, 61 °C) and denaturation (below, 97 °C). Therefore, there is no need of an external force to drive the fluid through different temperature zones, simplifying its operation and allowing the implementation of the desired number of thermal cycles.

3 Analysis Methods of Reaction Products

Following amplification, the identification of amplification products must be performed to read the results and/or to confirm that the correct product was generated. Analysis techniques that can be used should provide short analysis times, high sensitivity and specificity, and favorable LODs. A variety of analysis methods have been successfully demonstrated for microdevice examples, including μCE and DNA microarrays. While there are a number of alternative techniques for reading successful PCRs, we will restrict our discussion to these two particular techniques.

3.1 Microcapillary Electrophoresis

The operational advantages of μCE are the high separation efficiency, providing high specificity, and relatively short analysis times [148–151]. In narrow channels that possess the capacity to efficiently dissipate Joule heating, electric field strengths as high as 1 kV/cm can be used. Consequently, the analysis time is typically one order of magnitude shorter than that found in conventional slab gel electrophoresis (SGE). Another feature of μCE is that the operational conditions can be kept constant, defined, and reproducible by filling the separation channel with fresh electrolyte prior to each analysis. DNA separations employing μCE have undergone extensive development since its description and demonstration by Manz et al. [14] and Harrison et al. [152] in the early 1990s. These reports were followed by demonstrations of μCE for the high resolution separation of ssDNAs in chips consisting of many separation channels. For example, Woolley and Mathies [16, 153] reported DNA sequencing separations using a glass μCE device. DNA was introduced electrokinetically through an injection cross and separated on a 5-cm-long gel-filled microchannel in only 120 s (see Fig. 9). A brief description

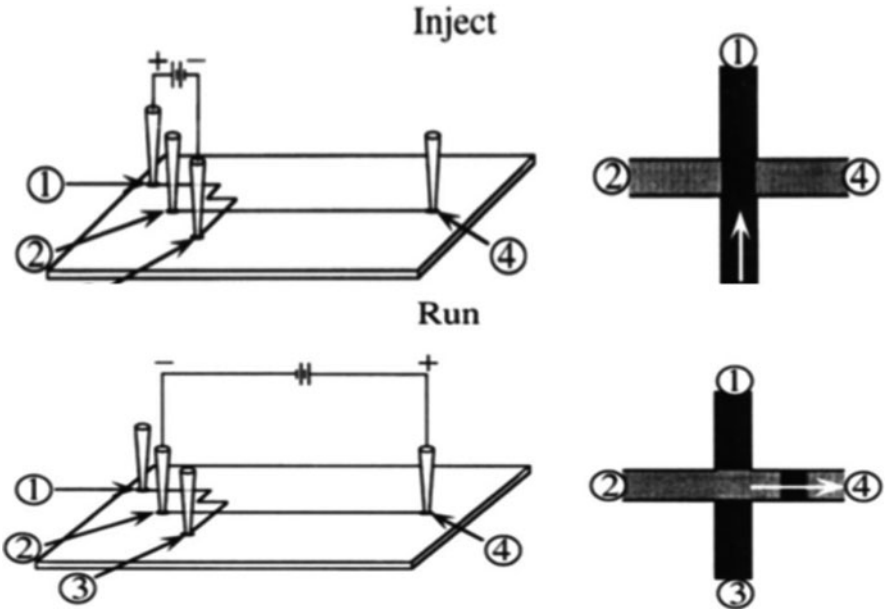

Fig. 9 Diagram of an electrophoresis chip indicating the injection procedure. The injection channel connects reservoirs *1* and *3* and the separation channel connects reservoirs *2* and *4*. In the injection mode (*top*), a field is applied between reservoirs *1* and *3* causing the DNA to migrate through the gel-filled intersection toward reservoir *1*. In the run mode (*bottom*), a field is applied between reservoirs *2* and *4* causing the DNA fragments in the intersection region to migrate toward reservoir *4* through the gel and into the separation channel. The actual device had 15 electrophoresis units integrated on each chip. Reproduced from [16] with permission

of μCE separation devices used for sorting DNAs will be described in Sects. 3.1.1–3.1.5 as well as a brief description of the fundamentals associated with CE in general.

3.1.1 Electrophoretic Mobilities

When a voltage is applied across a separation channel, the analyte migrates with an electrophoretic mobility and direction that generally depends on its chemical properties in the background electrolyte (BGE) and the applied electric field strength, E. The electric field strength is a ratio of the applied voltage (V) and the total capillary length (L_c) as shown in the following equation:

$$E = \frac{V}{L_c}. \tag{3}$$

By relating the velocity, v_{ep}, to E, the electrophoretic mobility (μ_{ep}) can be determined using:

$$\mu_{ep} = v_{ep}E^{-1} = q/(6\pi r\eta), \tag{4}$$

where q is the net charge on the analyte, r is the Stokes radius, and η is the viscosity of the BGE. It should be noted that the above equation is valid only for spherically shaped particles and must be modified for those molecules that adopt alternative configurations, such as DNAs.

Two electrically dependent phenomena contribute to the net mobility of an analyte, i.e., the intrinsic electrophoretic mobility and the electro-osmotic flow (EOF) [154]. The mobility can be evaluated from the electropherogram using the migration time, t_m, of the analyte migrating a distance L_d from the injection point to a detection point using:

$$\mu_{app} = \frac{L_d L_c}{t_m V} = \frac{L_d/t_m}{E}, \tag{5}$$

where μ_{app} refers to the apparent mobility, which accounts for the electrophoretic mobility of the analyte as well as the EOF.

In μCE, the EOF magnitude and direction depend on the charges present on the surface of the microchannel. For example, glass walls are negatively charged due to deprotonated silanol groups, which induce an EOF that travels from anode to cathode. The μ_{app} of an analyte inside a fused silica capillary or a microchannel that is superficially charged by contact with a solution typically consists of two contributions. The first is the electrophoretic movement of the analyte with respect to the electrolyte, which is characterized quantitatively by the effective mobility, μ_{eff}. The second contribution is the EOF of the liquid with respect to immobile, charged surfaces, which is characterized by μ_{eof} The net effective electrophoretic mobility (μ_{eff}) can be evaluated from the apparent mobility μ_{app} as follows:

$$\mu_{eff} = \mu_{app} - \mu_{eof}. \tag{6}$$

The μ_{eof} can be determined by using a neutral marker to determine t_{eof} from:

$$\mu_{eof} = \frac{L_d/t_{eof}}{E}. \tag{7}$$

We should note that in most DNA electrophoretic separations, the EOF is typically suppressed using either linear polyacrylamides covalently attached to the separation channel wall or dynamic coatings. Therefore, due to the fact that DNAs are polyanionic, they will exclusively migrate from cathode to anode, requiring that the electrophoresis analysis should be operated with the injection end cathodic.

3.1.2 Separation Selectivity

Separation selectivity, S, in electrophoresis is defined as the effective mobility difference between two migrating components [155], and is expressed as:

$$S = \frac{\Delta\mu_{\text{eff}}}{\mu_{\text{av}} + \mu_{\text{eof}}}, \tag{8}$$

where μ_{av} is the average of the effective mobilities. For closely migrating analytes, the average effective mobilities may be replaced by the effective mobility of one component [156].

3.1.3 Resolution

The resolution of two components can be determined from [157]:

$$R = \frac{L_{\text{c}}(\mu_{\text{eff1}} + \mu_{\text{eff2}})}{4\mu_{\text{eff1}}\left[\left((\mu_{\text{eff1}} E_{\text{inj}} t_{\text{inj}})^2/12\right) + (2DL/\mu_{\text{eff1}} E)\right]^{1/2}}, \tag{9}$$

where L_{c} is the channel length, μ_{eff1} and μ_{eff2} are the effective mobilities of the two components of interest, E_{inj} is the electric field applied to perform injection, t_{inj} is the injection time, and D is the average diffusion coefficient of the components. Depending on which of two regimes is operating, the resolution depends on either the length of the channel or the square root of the length. In the first regime, band broadening due to electrokinetic injection dominates and the resolution scales with length. In the second regime, diffusion contributes primarily to band broadening, resulting in a square root dependence of R on length. The contribution of the electrokinetic injection to band broadening can be reduced by microfabrication and in conjunction with control of voltages on channel arms for determining the shape and size of the injected plug for short separation lengths [158].

3.1.4 DNA Separation Matrices

Size-based separations of homogeneous polyelectrolytes, such as DNA, are not possible in free solution electrophoresis [159]. This is due to the proportionality of the friction hydrodynamic force and total charge of the molecule to its length. The friction hydrodynamic forces exerted on the free-drained polymer coil while it moves as well as the accelerating electrostatic force both increase proportionally with the addition of a nucleotide to the chain. This is why one must typically use a sieving media, such as a gel or an entangled polymer solution, to obtain size-based separations of DNA using electrophoresis.

DNA electrophoretic mobilities are highly dependent on the nature of the matrix in which the separation takes place. For example, in free solution, the DNA molecules migrate with a mobility that is independent of size [160, 161], because the charge per unit mass is the same for all DNA molecules. However, the mobility becomes dependent on molecular mass in sieving gels. The mobility in sieving gels

is related to the fractional volume $f(C)$ of the matrix available to the migrating DNAs according to:

$$\frac{\mu}{\mu_0} = f(C), \tag{10}$$

where, μ is the mobility observed in the matrix, μ_0 is the free solution mobility and $f(C)$ is the available fractional volume in the gel or entangled polymer solution [162]. If the sieving mechanism in the matrix is similar to that described by Ogston [163], $f(C)$ is related to gel concentration, C, as shown in the following:

$$\frac{\mu}{\mu_0} = f(C) = \mathrm{e}^{-KC}, \tag{11}$$

where K, the retardation coefficient, is dependent on the macromolecule size [164, 165]. Plots of the logarithm of μ/μ_0 as a function of gel concentration are known as Ferguson plots [166]. Linear Ferguson plots indicate that the separation takes place in the Ogston regime, where the average pore radius of the gel is larger than the radius of gyration of the migrating macromolecule. DNA mobilities in various sieving media are determined by the interplay of three factors: (1) the relative size of the DNA molecule with respect to the effective pore size of the matrix; (2) the effect of the electric field on the matrix; and (3) specific interactions of DNA with the matrix during electrophoresis [167].

Many different polymers have been investigated as separation matrices, including liquefied agarose, cellulose derivatives, dextrans, linear polyacrylamides (LPA) and their derivatives, poly(ethylene oxides) (PEO) and polyvinyl alcohols. The solution properties of these polymers are described elsewhere [168–176]. Most of these polymers provide good separations in certain DNA mass ranges [174, 175, 177]. For example, Njoroge et al. [178] used a 4% w/v LPA gel of ~6.6 MDa as a sieving matrix in a poly(methyl methacrylate) (PMMA) μCE device and achieved favorable resolution of PCR fragments of forensic *Alu* elements varying over a large size range (199–887 bp). The LPA was suspended in 1× TTE that contained 0.05% (w/v) methyl hydroxyethyl cellulose (MHEC) for EOF suppression in the PMMA device, and 7 M urea to denature the DNA. Using this matrix, PMMA microchip separations provided near-baseline resolution for all 20 components of a 900-bp sizing ladder. The separation of large DNA has been improved in sparsely crosslinked "nanogels" by ~10.4% compared to separation in LPA [179]. Nanogels are synthesized by incorporating a low percentage (~10^{-4} mol%) of *N*,*N*-methylene bisacrylamide crosslinker in LPA of high molar mass [180].

For polymers of comparable molar mass, hydrophilic polymers form more highly entangled networks because each molecule occupies a relatively large volume in solution [176]. The major differences between DNA separations in slab gels and entangled polymer solutions is that the entangled polymers are free to move about in the solution [181], creating dynamic pores in the matrix as they change interacting partners. The movements of the polymer chains give rise to

a process called constraint release, which increases the mobility of the DNA [182–184].

3.1.5 End-Labeled Free-Solution Electrophoresis

Mayer, Slater, and Drouin [185] were the first to quantitatively examine end-labeled free-solution electrophoresis (ELFSE), also referred to as free-solution conjugate electrophoresis (FSCE), for the potential of sorting DNA in free solution without requiring a sieving matrix. Their theoretical model was based on two assumptions: The first was that the velocity of a hybrid ELFSE molecule (made of a charged component, the DNA fragment, and an uncharged component, the drag-tag) is given by the total electrical force applied to the molecule divided by the total friction coefficient of a free-draining molecule. The second assumption was that, in free solution, the Einstein relation [186] should relate the diffusion coefficient, $D(M)$, to the electrophoretic mobility, $\mu(M)$, of a DNA molecule of size M [see (14)].

In free solution, a DNA molecule of M bases behaves as a free-draining coil, and its $\mu(M)$ is independent of M. However, labeling the DNA with a molecular species having a different charge-to-friction ratio can lead to a size-dependent mobility. By neglecting the eventual electrostatic and hydrodynamic interactions between the DNA and the friction-generating label, the free-solution mobility of the end-label–DNA complex simply equals its charge-to-friction ratio, which is calculated from the following equation:

$$\mu(M) \approx \frac{\rho(M-\beta)}{\xi(M+\alpha)} = \mu_0 \frac{(M-\beta)}{(M+\alpha)}, \tag{12}$$

where α is the friction due to the end-label, ξ is the friction of one base, $-\beta$ is the effective charge carried by the end-label (the negative sign in front of β arises from the fact that DNA is negatively charged), ρ is the electric charge carried by one base, and $\mu_0 = \rho/\xi$, which is the free-solution mobility of a normal free draining DNA molecule. This equation shows that the mobility of an end-labeled DNA complex is now a function of the size of the DNA fragment when $\alpha \neq -\beta$ and the separation is possible with end-labels having a charge-to-friction ratio that is different from the charge-to-friction ratio of DNA (in practice, $M > \beta$ is also required to ensure that all the molecules migrate in the same direction). In ELFSE, the $\mu(M)$ of a DNA fragment can also be determined from the following equation:

$$\mu(M) = \frac{\mu_0}{1 + \alpha/M}. \tag{13}$$

In contrast to classical gel electrophoresis, complexes containing long DNA fragments will have higher velocities than complexes containing short DNA fragments [185]. By considering the Brownian diffusion as a source of band broadening

only in free solution, the Einstein relation [186] should relate $D(M)$ to $\mu(M)$ as shown in the following expression:

$$D(M) = \frac{\mu(M)k_{\mathrm{B}}T}{\rho(M-\beta)} = \frac{\mu_0 k_{\mathrm{B}}T}{\rho(M+\alpha)}, \tag{14}$$

where k_{B} is the Boltzmann constant and T is the temperature. By assuming that consecutive end-labeled DNAs have the same intensity and a Gaussian shape, the minimum migration distance, $L_{\min}(M)$, required to separate molecules differing in length by a single base is approximately derived from:

$$L_{\min}(M) \approx \pi r^2 \frac{S\mu(M)D(M)}{E\left(\frac{\partial\mu(M)}{\partial(M)}\right)^2}\left(1 + \left[(1+\gamma^2)^{1/2}\right]\right), \tag{15}$$

$$\gamma = \frac{\omega_0 E}{(S)^{1/2}D(M)} \times \frac{\partial\mu(M)}{\partial(M)},$$

where ω_0 is the peak width, and S is a numerical factor of order unity and depends on the efficiency of the detection method [185].

As a proof of concept, Heller et al. [187] used ELFSE for the separation of double-stranded DNA (dsDNA) fragments by free-solution CE. The drag-tag was added to the DNA fragments using a method similar to that previously used to study DNA migration in polyacrylamide gels and polymer solutions [188–190]. The results shown in Fig. 10 confirmed the predictions [185] that in the absence of EOF, the end-labeled molecules with longer DNA segments migrate faster than the shorter ones, and that higher resolution could be observed with a larger label or, in this case, with two labels instead of one. Using the original Mayer et al. [185] ELFSE theory to fit the data, the relative friction coefficient, α, for a streptavidin drag-tag can be estimated by the slope of the straight line obtained from plotting μ_0/μ^{-1} versus $1/M$ (see inset in Fig. 10). Using the data of Fig. 10, it was estimated that adding a single streptavidin drag-tag generated a friction equivalent to ~23 uncharged nucleotides, whereas adding two streptavidins generated a friction equivalent to 54 uncharged nucleotides (inset in Fig. 10a). The potential of this technique has been demonstrated by the separation of DNA sequencing fragments [191] and detection of single-nucleotide polymorphisms using electrophoresis [192].

Sinville et al. [193] combined an allele-specific ligase detection reaction (LDR) with FSCE (LDR–FSCE) for multiplexed electrophoretic screening of low-copy number mutations in a high abundance of wild-type DNA using PMMA microchip devices. To conduct FSCE separations of LDR-drag tags products, the LDR discriminating primers were reconfigured to allow for the addition of drag-tags onto their 5′ terminus. Using a dynamically coated separation channel, the PMMA

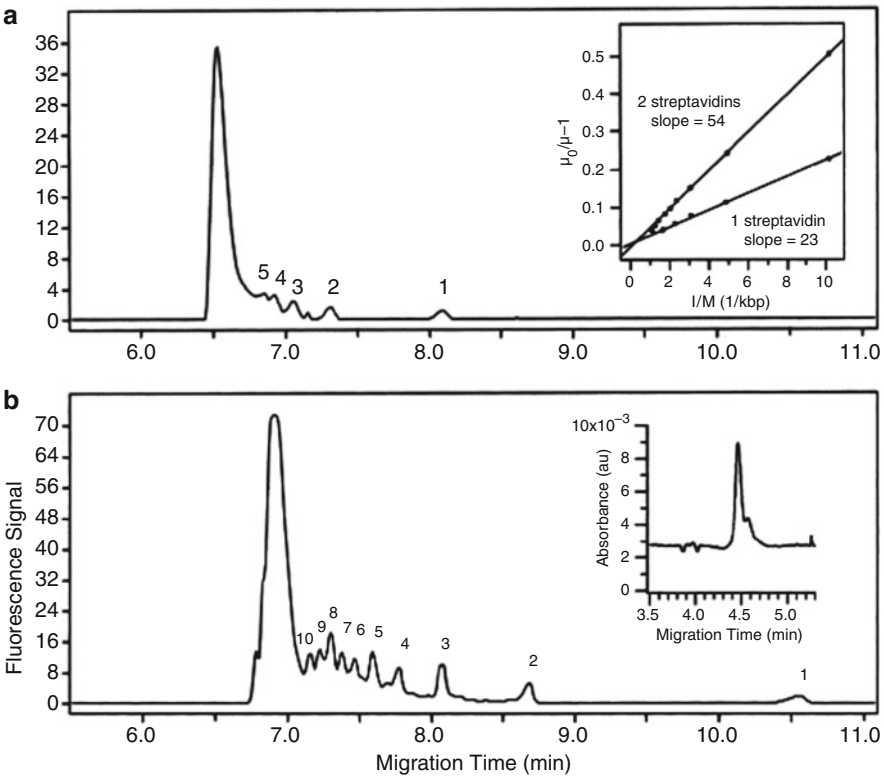

Fig. 10 Separation of a 100-bp dsDNA ladder with (**a**) one or (**b**) two streptavidin molecules used as ELFSE drag-tags. The peaks marked *1–10* represent the 100–1,000 bp dsDNA fragments, respectively. *Inset* in (**a**): plot of μ_0/μ^{-1} vs. 1/*M*. *Inset* in (**b**): polydispersity of streptavidin as measured by CE. Reproduced from [187] with permission

μCE device achieved simultaneous detection of four mutant alleles in ~85 s, which was >7.5 times faster than a commercial capillary system.

3.2 DNA Microarrays

DNA microarrays were first developed in the early 1990s [194–196] and have become an important tool for high-throughput DNA analysis. A DNA microarray consists of a collection of oligonucleotide probes attached to a solid support in an orderly manner, typically a two-dimensional array. The probes readily hybridize to amplified gene fragments (targets) that are complementary to a specific probe. Readout of successful hybridization events is accomplished using a fluorescent dye or other such label attached covalently to the target. The mRNA expression

levels or DNA sequence variations from hundreds to thousands of genes can be interrogated simultaneously. A few recent reviews of microarray technology are recommended to interested readers [197–201].

The basic elements required for the DNA microarray are the solid substrate, the attachment chemistry of the probe to the solid support, the approach adopted to "spot" the probes at particular locations of the two-dimensional array, the method employed to bring the solution target to the appropriate location of the array (passive or active), and the readout modality. A brief discussion of some of these important elements is given in Sects. 3.2.1–3.2.3.

3.2.1 Substrate Materials for Microarray Construction

A variety of solid substrates have been explored for microarrays, such as glass [202, 203], polymers [69, 98, 204–212], gold [213], optical fibers [214], and microbeads [215, 216]. Several issues must be considered in choosing the appropriate substrate, including the level of scattering and fluorescence background generated from the substrate, its chemical stability and complexity, the amenability to modification or derivatization of the substrate, loading capacity, and the degree of nonspecific interactions [202]. Glass has been widely adopted as a substrate material due to its favorable optical properties, which are highly desired for signal readout of the microarray using fluorescence. However, the microarray fabrication process involved for glass uses siloxane chemistry to tether oligonucleotide probes to the glass. These siloxane linkages are susceptible to hydrolytic cleavage, especially at extreme pH values. Recently, polymers have been used as alternative microarray substrate materials because of their diverse properties that can be selected to suite different immobilization strategies of probes to the substrate, and the ability to microfabricate structures in a low cost, mass-production mode for single-use applications. Polymers that have been used for microarray applications include PDMS [204, 205], PC [69, 98, 206], PMMA [207–211], and polystyrene [212].

The use of microbeads as substrates for the immobilization of oligonucleotide probes has also been reported. Fan and coworkers [215] described a dynamic DNA hybridization approach using paramagnetic beads as a transportable solid support. DNA targets were immobilized onto beads via streptavidin–biotin linkages for interrogation with probes that were transported via pneumatic pumping. Their experiment showed that beads containing DNA targets could be sequentially interrogated up to 12 times with no measurable change in the hybridization signal. Ali et al. [216] demonstrated a chip-based array composed of avidin-coated agarose microbeads for the discrimination of single-nucleotide mismatches. In their work, the biotinylated oligonucleotide probes containing microbeads were selectively arranged in micromachined cavities localized on silicon wafers, and the fluorophore-conjugated DNA target was a complement to the probe. The microcavities possessed *trans*-wafer openings allowing for both fluid flow through the bead chambers and optical analyses at numerous bead sites. Hybridization times on the

order of minutes, with point mutation selectivity factors greater than 10,000 and an LOD of 10^{-13} M were achieved using this microbead array.

3.2.2 Surface Modification for the Immobilization of Probes

Various surface modification strategies have been used to attach probes to different solid supports. Oligonucleotide probes can be electrostatically attached to polylysine-derivatized or amino-silanized glass slides, representing a noncovalent approach [217]. Probes can also be covalently linked to the surface of the array by brief exposure to UV light [218]. Biotinylated DNA probes can be attached to streptavidin-coated magnetic beads [215], or thiol-terminated oligonucleotide probes can be immobilized to gold.

Methods for the end attachment of chemically modified oligonucleotide probes to a solid substrate have been reported as well. For example, Joos et al. [203] developed the covalent attachment of amine-terminated oligonucleotide probes to a glass substrate. Glass slides were derivatized with aminophenyl or aminopropyl silanes, and amine-terminated oligonucleotides were attached to the silanized glass with a crosslinking reagent such as glutardialdehyde. Using this approach, up to 90% of the attached oligonucleotides were available for hybridization.

Lenigk and coworkers [206] demonstrated the use of bifunctional linkers for the immobilization of amine-terminated oligonucleotide probes. In their work, a PC surface was coated with a photosensitive polymer (SurModic's photoreactive reagents) followed by 60 s UV irradiation to generate functional groups that allowed amine-terminated oligonucleotide probes to be covalently attached onto the surface. Detection of four pathogenic bacteria surrogate strains from multiple samples was accomplished using this device.

Wang et al. [207] reported the covalent attachment of amine-terminated oligonucleotide probes to a chemically modified PMMA substrate. In their protocol, the PMMA surface was aminated using a *N*-lithioethylenediamine solution, where methyl-ester functional groups were replaced by *N*-lithioethylenediamine. After aminolysis, the surface was activated with a homo-bifunctional crosslinker, glutardialdehyde, via a Schiff's base reaction and was converted to an aldehyde-terminated surface, which allowed for the covalent attachment of oligonucleotide probes. They found that the oligonucleotide coupling chemistry allowed reuse of the array >12 times without significant hybridization signal loss.

McCarely et al. [219, 220] described a simplified photomodification protocol of PMMA and PC substrates through direct and controlled UV exposure of the substrates in an oxygen-rich environment to yield surface carboxylic acid moieties. Patterns of carboxylic acid sites could be formed by exposure of the polymers in air to UV irradiation at 254 nm with a power density of 15 mW/cm^2 for ~60 min without significant physical damage to the polymer surface. The so-formed chemical patterns allowed for further functionalization to yield arrays or other structured architectures through covalent attachment chemistry.

Soper et al. [211] presented the fabrication of DNA microarrays onto PMMA surfaces using a UV modification protocol as shown in Fig. 11. Briefly, the PMMA surface was first activated via exposure to UV irradiation, which produced carboxylic acid functional groups onto its surface. EDC/NHS coupling chemistry was then used to facilitate the formation of succinimidyl ester intermediates on the surface, which allowed for the covalent attachment of amine-terminated

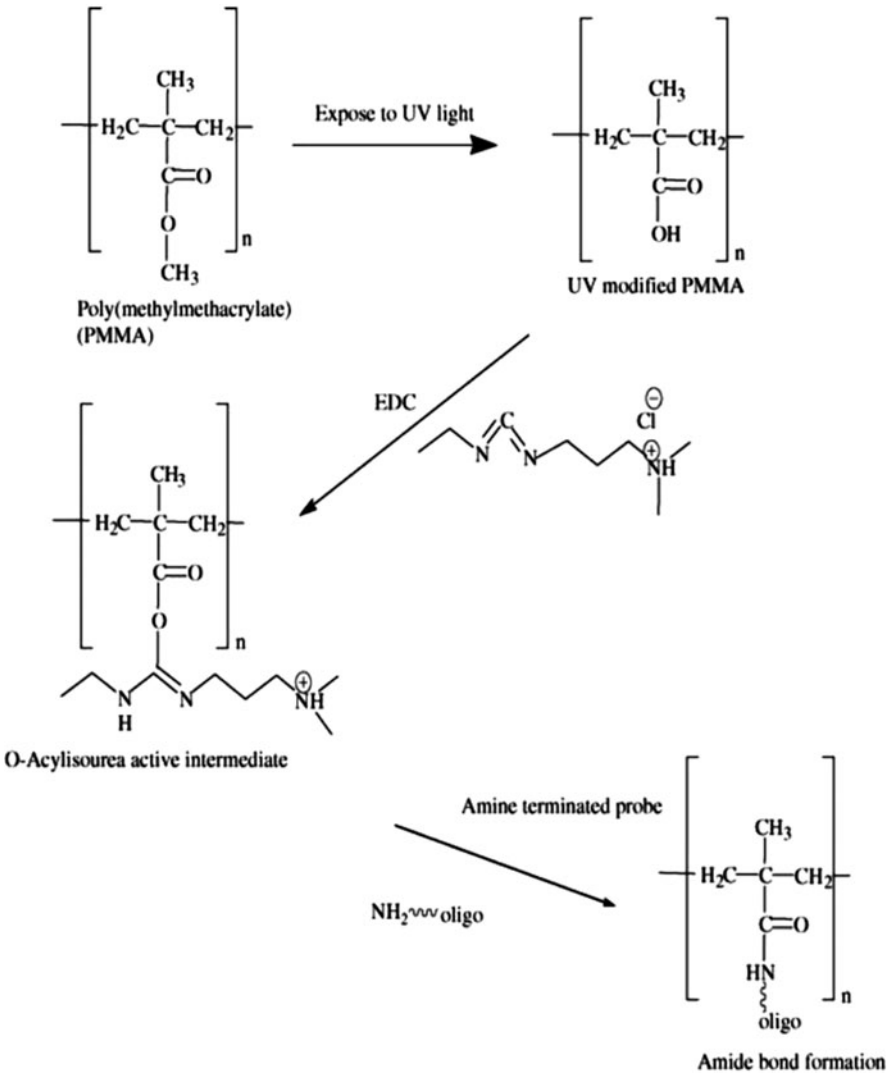

Fig. 11 UV activation of PMMA forming surface-confined carboxylic acid groups with the subsequent attachment of 5′ amine-containing oligonucleotides. Reproduced from [211] with permission

oligonucleotide probes. Recently, this same group enhanced the density of surface carboxylate groups by utilizing oxygen plasma treatment to create low density arrays on the surface of a free-standing, air-embedded PMMA waveguide [209].

3.2.3 Hybridization Efficiency Improvements

Merging microarrays to microfluidics is a step toward building integrated microfluidic systems for genetic analysis. In addition, it can provide significant reductions in target and probe hybridization reaction times resulting from diffusion-limited hybridization kinetics. Compared to a conventional two-dimensional hybridization array in a 1×1 cm format, hybridization occurring within a microfluidic channel significantly reduces the diffusional distances between the target molecules and the probes immobilized onto the surface. Shuttling back-and-forth, the hybridization mixture inside a microchannel can further facilitate mass transport and, thus, reduce hybridization time. Examples demonstrating improvements in hybridization efficiency using microfluidics have been reported [204, 205, 207, 221–224].

Liu and Rauch [221] investigated DNA hybridization in a microfluidic channel fabricated from a variety of plastic materials. By oscillating the hybridization mixture in the microfluidic channel, maximum signal was observed within a hybridization time of 15 min. Wang et al. [207] reported a low density array constructed inside a PMMA microfluidic device and used flow-through feed of the hybridization mixture, which successfully reduced the hybridization time from ~5 h to 1 min and reported an LOD of 10 pM for the identification of low abundance point mutations (one mutant in 10,000 wild-type DNA molecules) found in a K-*ras* oncogene. Erickson et al. [204] developed a theoretical model for electrokinetically controlled DNA hybridization in microfluidic devices, which predicted that reducing the height of the microchannel would effectively accelerate the diffusion-limited reaction kinetics and reduce the time required for the hybridization reaction to reach steady state. Following numerical simulations, the experimental results indicated that all processes from sample dispensing to hybridization detection could be completed within 5 min inside a glass–PDMS microchannel with a height of 8 μm. Yuen and coworkers [205] fabricated a microfluidic device consisting of two interconnected reaction chambers molded in PDMS on a standard microscope slide for closed-loop fluidic circulation and mixing. Fluid samples were circulated and mixed by the rotation of a magnetic stirring bar driven by a standard magnetic stirrer. A two- to fivefold increase in hybridization efficiency was observed with fluid circulation. Wei et al. [222] described the use of discrete sample plugs in a hybrid glass/PMMA microfluidic device for droplet hybridization (see Fig. 12). In this case, plugs were shuttled back and forth inside a channel sweeping over the probes, which were thoroughly mixed by the natural recirculating flows, significantly reducing the hybridization reaction volume to 1 μL. The total reaction time was 500 s, and the LOD was 19 amol.

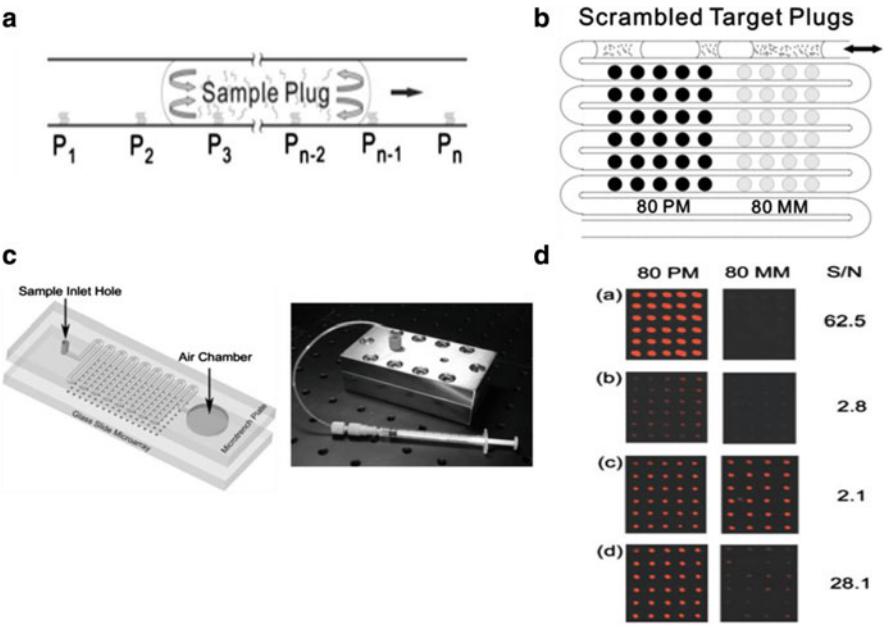

Fig. 12 (**a**) Droplet shuttle hybridization in a microchannel. P_1, $P_2 \ldots P_n$ refer to the probe spots. (**b**) Illustration showing that scrambled discrete plugs sweep over different probes in the channel. *80 PM* and *80 MM* denote the perfect match and mismatch probes, respectively. (**c**) Microtrench plate is stacked on a glass microarray slide (*right*) with a photograph of the assembled device (*left*). (**d**) Signal-to-noise (*S/N*) ratios for various hybridization formats: *1* shuttle hybridization at 500 s, sample volume 1 μL; *2* static microfluidic hybridization at 500 s, sample volume 10 μL; *3* flat glass hybridization at 500 s, sample volume 30 μL; and *4* flat glass hybridization at 18 h, sample volume 30 μL. The target concentration is 90 nM. The *left column* presents the fluorescence images with 80 PM probe, and the *right column* presents the fluorescence images with 80 MM probe. Reproduced from [222] with permission

4 Integrated Microfluidic Systems

The integration of sample pretreatment with analytical processing steps for the analysis of biological samples has remained the primary goal of μTAS as described by Manz and coworkers [14] over two decades ago. Many of these visions are becoming a reality and some of these systems will be described here. As noted previously, genetic analysis systems are defined as a single wafer or a collection of wafers seamlessly interconnected that possess two or more processing steps for the analysis of a genetic sample. Genetic analysis encompasses a large number of different types of applications, for example, DNA forensics where unique genetic markers are used for human identification either at crime scenes or in battlefields. For in vitro diagnostics, mutations in certain gene fragments can be detected and used to discover the presence of a disease in a particular patient, and also provide

information to the clinician on how to treat that patient. In Sects. 4.1 and 4.2 we will discuss systems that include the sample preprocessing functions followed by either μCE or microarray readout of the preprocessing steps.

4.1 Integrated Systems with μCE Readout

The analytical challenge in coupling μCE with front-end sample preprocessing is the integration of pressure-driven flows required for the front-end with electrokinetically driven flows required for the back-end. In addition, the presence of any residual hydrodynamic flow during the separation can degrade separation efficiency due to the parabolic flow profile that is generated, compared to plug flow for electrokinetic flow. As such, the integration challenge in microfluidics is interfacing PCR with μCE separation because of sample transfer from hydrodynamic to electrokinetic flow. The quality of a separation depends, in part, on successful injection processes. The contribution of the injection process to the height equivalent of a theoretical plate H can be estimated from the following equation [225]:

$$H = \frac{L_{\text{sample}}^2}{Kl}, \tag{16}$$

where L_{sample} is the length of the sample plug along the separation channel, K is the injection profile factor, and l is the separation length (distance between injection and detection points). The injection profile factor reflects the peak shape of sample plug during injection and depends on the injected volume, the injector geometry, and the method of injection, and can vary between 1 for an exponential-decay injection and 12 for an ideal sample plug [226, 227]. This implies that the contribution of a specific injector to the total band broadening may vary by more than a factor of 10.

The injection step usually involves several intersecting channels and many injection designs have been developed and reviewed [228]. Most designs use cross- or double-T intersections, proposed initially by Harrison et al. [229, 230] and Effenhauser et al. [231, 232], respectively. For each injection design, different injection modes can be employed depending on the electric field sequences and distributions [233]. The three major limitations for electrokinetic injection are:

1. It is biased toward small DNA fragments with high electrophoretic mobility thereby complicating injection optimization. For example, unpurified PCR products contain high concentrations of salt and an excess of short unreacted primers, which can lead to long loading times.
2. The injected sample is small (<1% of the total sample volume), which imposes unavoidable restrictions on the sensitivity and quantitation of the analysis [234, 235].
3. The injection time becomes highly variable when one is injecting limiting amounts of analyte from nanoliter volumes [5, 54].

The injection methods used in μCE can either be stacking- or extraction-based methods. Stacking methods such as mediated stacking [236], gated injection [237], field amplified sample injection [238], the staggered-T configuration [239], field-amplified sample injection [238], and pressure-driven injection [10, 86] are widely adopted in μCE because they are simple to implement. Extraction-based techniques, such as membrane filtration [240, 241], SPE [32, 242], liquid–liquid extraction [243], and bioaffinity purification [53, 244] offer a more scalable platform for complete sample injection.

One of the first reports of an integrated microchip for DNA analysis was reported in 1998 by Burns and colleagues [245], which included a resistive heating region for DNA amplification, a sample loading region, and a gel-based separation region. This work utilized a single-strand displacement assay [246] with other sample analysis steps on one device. The system (see Fig. 13a) was fabricated entirely in Si using standard photolithography and consisted of devices for nanoliter sample injection, mixing of reagents, amplification or enzymatic digestion of the DNA sample, gel electrophoresis and, finally, fluorescence detection. The only components not situated on the chip were the fluorescence excitation source, pressure source, and control circuitry. Figure 13b shows the fluorescence image of a 50-bp ladder separated using μCE with a polyacrylamide gel. The system was demonstrated to perform an isothermal amplification of DNA using strand displacement amplification with the DNA target stained with SYBR green.

Waters et al. [20] reported a system that was micromanufactured in glass and consisted of a rather simple architecture: the microchip used a reservoir machined into the glass as a reaction chamber to perform, sequentially, cell lysis and a multiplex PCR amplification. The chip was fabricated using photolithography and wet chemical etching of the glass substrate. The monolithic chip was placed directly onto a commercial thermal cycler to allow thermal processing of the sample. Following PCR, the products were directly injected using a cross-T injector in a μCE channel and separated in a 1% hydroxyethyl cellulose (HEC) sieving matrix for size separation. An intercalating dye was used for the fluorescence detection of the generated DNA fragments.

Obeid and coworkers [128] reported a microsystem fabricated on two glass plates (each 40 × 45 × 0.55 mm), where a continuous channel network was etched into the bottom plate by standard photolithography and wet chemical etching, followed by thermal fusion-bonding of the two plates to form a closed structure. This system (see Fig. 14a) used a continuous flow concept to demonstrate functional integration of reverse transcription (RT) and PCR (RT-PCR) with operator selection of the number of amplification cycles to secure the results shown in Fig. 14b. The RT phase of the measurement involved the synthesis of DNA using mRNA templates and was performed before DNA amplification to allow quantification of mRNAs. The integration of RT and PCR processes within a monolithic chip is often problematic as RT components can interfere with the subsequent PCR [59]. Obeid and colleagues[128] tackled this problem by reducing the flow rate at which reverse transcription was performed so that at the intersection of the RT and PCR channels, the RT mixture constituted only ~10% of the total PCR volume.

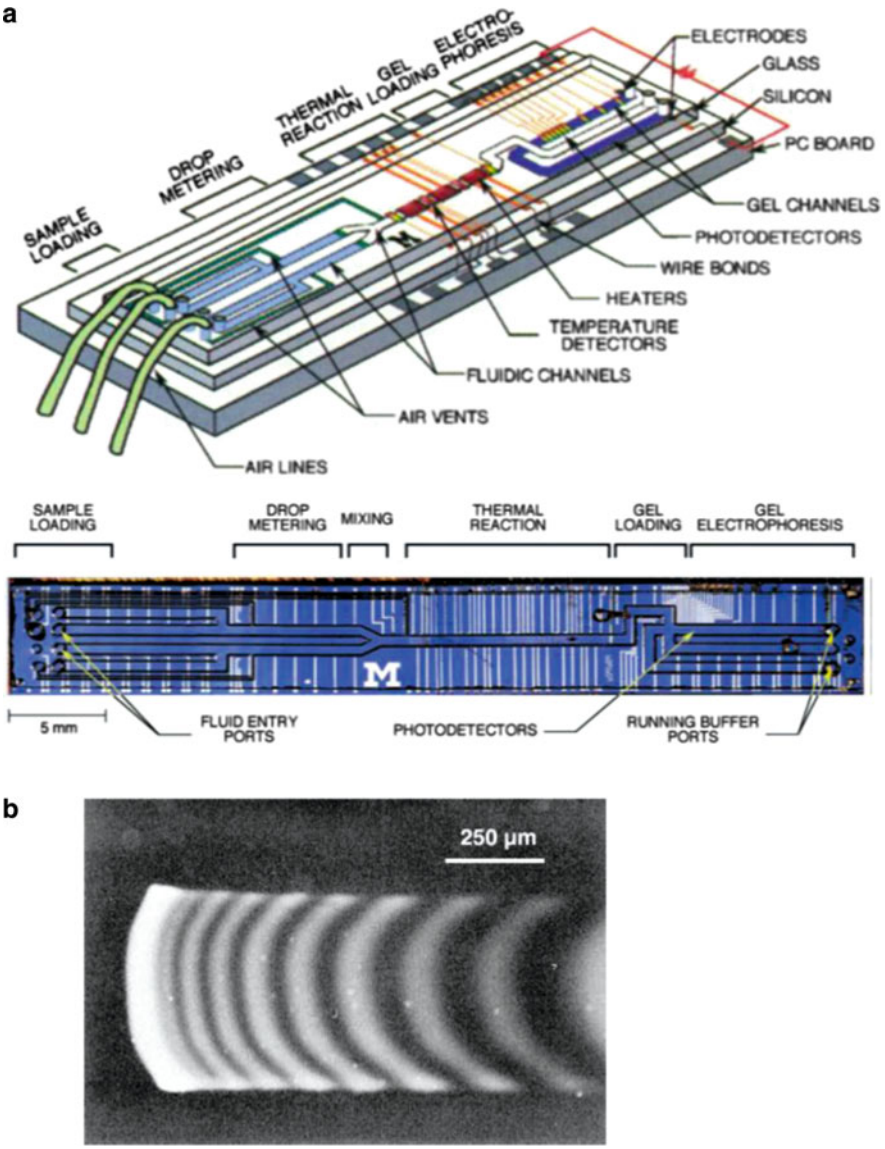

Fig. 13 (**a**) Integrated DNA analysis system developed by Burns and coworkers [245]. The device was made on a Si substrate and included the following elements: fluidic channels, heaters, temperature sensors, and a fluorescence detector to monitor the generation of DNA products. The following functions were incorporated into the system: mixing of solutions, amplifying or digesting DNA, separating the products using µCE, and detecting these products directly on-chip. *Blue* liquid sample, *green* hydrophobic surfaces, *purple* polyacrylamide gel. The *bottom panel* shows an optical micrograph of the device from above. (**b**) Optical micrograph of a 50-bp DNA ladder sorted in a 500-µm-wide polyacrylamide gel. Reproduced from [245] with permission

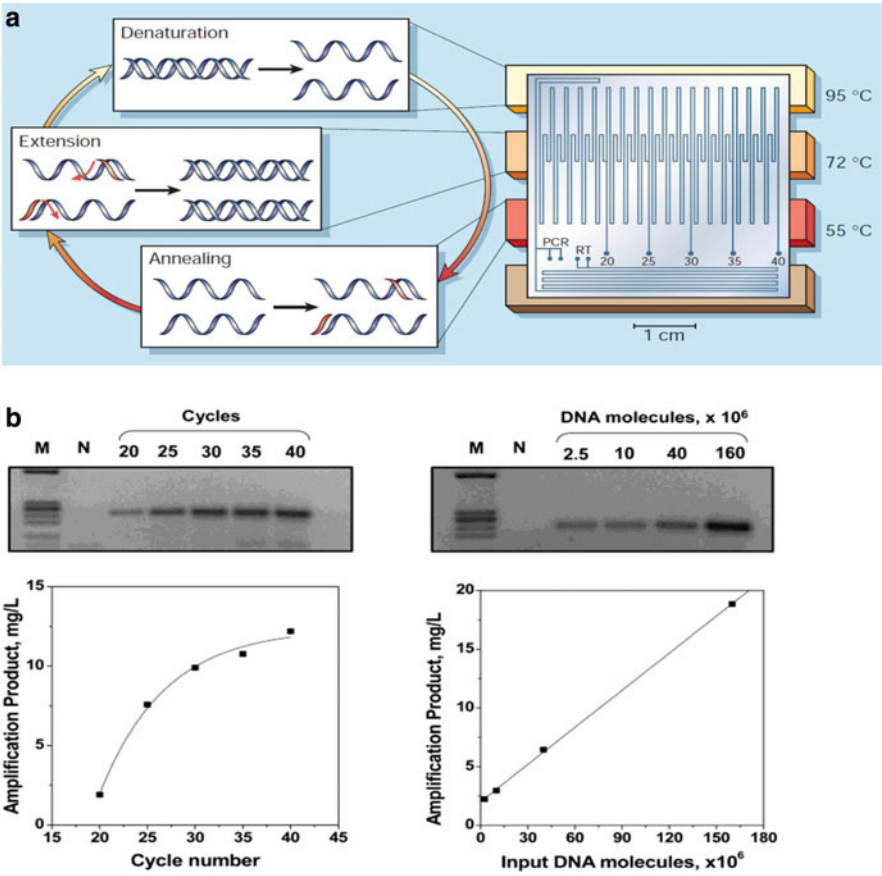

Fig. 14 (**a**) Microfabricated device for CFPCR and RT-PCR in which DNA can be amplified quickly using the PCR. When a sample is added at either of the PCR inputs, it flows over heating blocks whose temperatures are set to induce the three steps of PCR consecutively: denaturation, annealing of the PCR primers, and extension of the primers into complete DNA strands producing two copies of the original DNA strand. Samples can be extracted from the chip between 20 and 40 PCR cycles at the points indicated. (**b**) *Left*: Effect of the cycle number on the concentration of amplification product in CFPCR with on-chip cycle selection. The input DNA was 10^7 molecules. *Right*: Study of the concentration of the amplification product as a function of the input DNA molecules. All products were collected at 30 cycles. A 0.23-kbp PSA DNA template was used. *M* DNA markers. *N* negative (no DNA template). Reproduced from [128] with permission

The system was demonstrated by performing an amplification of the β-globin gene from human genomic DNA isolated from whole blood. The RT-PCR products were analyzed off-chip using agarose gel (2%) electrophoresis and ethidium bromide staining.

Soper and colleagues [208] investigated the effect of carryover from a primary PCR on a subsequent LDR in terms of LDR yield and fidelity using a continuous flow system microstructured on a PC substrate. Using this PC chip, three steps were

carried out: (1) amplification of the gene fragments from genomic DNA using PCR; (2) mixing of the resultant PCR product(s) with an LDR cocktail via a Y-shaped passive micromixer (see Fig. 15); and (3) ligation of two primers for detection of mutant DNA in an excess of wild-type sequences (1:1,000 mutant:wild type). It was found that a post-PCR treatment to deactivate *Taq* polymerase prior to the LDR phase of the assay was not essential [247]. The PCR/LDR continuous flow microsystem was demonstrated by detecting single nucleotide polymorphisms in *KRAS* genes, which carry high diagnostic value for colorectal cancers. The PCR/LDR products were analyzed off-chip using polyacrylamide gel electrophoresis and ethidium bromide poststaining.

Wang et al. [52] reported a CFPCR chip that consisted of a 20-loop spiral microfluidic channel hot-embossed into a PC substrate. The CFPCR chip was interfaced to a solid phase reversible immobilization (SPRI) chip made from UV-activated PC for purification of Sanger DNA sequencing ladders produced in the CFPCR chip. The CFPCR chip had three well-defined temperature zones poised at 95, 55, and 60°C for denaturation, renaturation, and DNA extension, respectively. The system was demonstrated for Sanger cycle sequencing using dye-terminator chemistry. The CFPCR-SPRI system could prepare a sample for electrophoretic sorting in less than 30 min. Following CFPCR-SPRI processing, the purified products were collected into a microtiter plate and directly introduced into a conventional capillary gel electrophoresis machine for separation and automated base calling. Average read lengths of 682 bases with a 99% calling accuracy were reported.

Lagally et al. [79] developed a fully integrated genomic analysis microsystem that included microfabricated heaters, temperature sensors, and 200 nL PCR chambers directly connected to μCE. The system was microstructured using a hydrofluoric acid etching procedure for glass as described by Simpson et al. [248]. The system was also equipped with PDMS valves and hydrophobic vents to provide controlled and sensorless sample positioning into PCR chambers connected to electrophoretic separation channels. The use of microfabricated heaters and temperature sensors created uniform heating over the entire PCR chambers and fast thermal response times, while minimizing power requirements. The heating and cooling rates for the PCR were 20 °C/s and the 20 PCR cycles were completed in 10 min. The ramp rates were within the range reported for devices in which the heating elements are in contact with the PCR chambers [20, 64, 66, 75, 117, 249, 250], but slower than rates reported for noncontact devices [134, 251].

Koh et al. [9] demonstrated a microsystem fabricated using a poly(cyclic olefin) substrate, which was produced by first creating the desired pattern on a glass plate using photolithography and wet etching. A layer of metal (100 μm–1 mm) was then electroplated onto the surface of the glass plate to create a molding tool (an electroform) from which microstructures were embossed into a poly(cyclic olefin) resin using compression molding. The resulting microsystem contained a cell thermal lysis unit along with integrated valves, which could withstand pressures up to 100 psi, and a PCR device that was directly connected to a CE microchannel to sort fluorescently labeled PCR products generated from different strains of

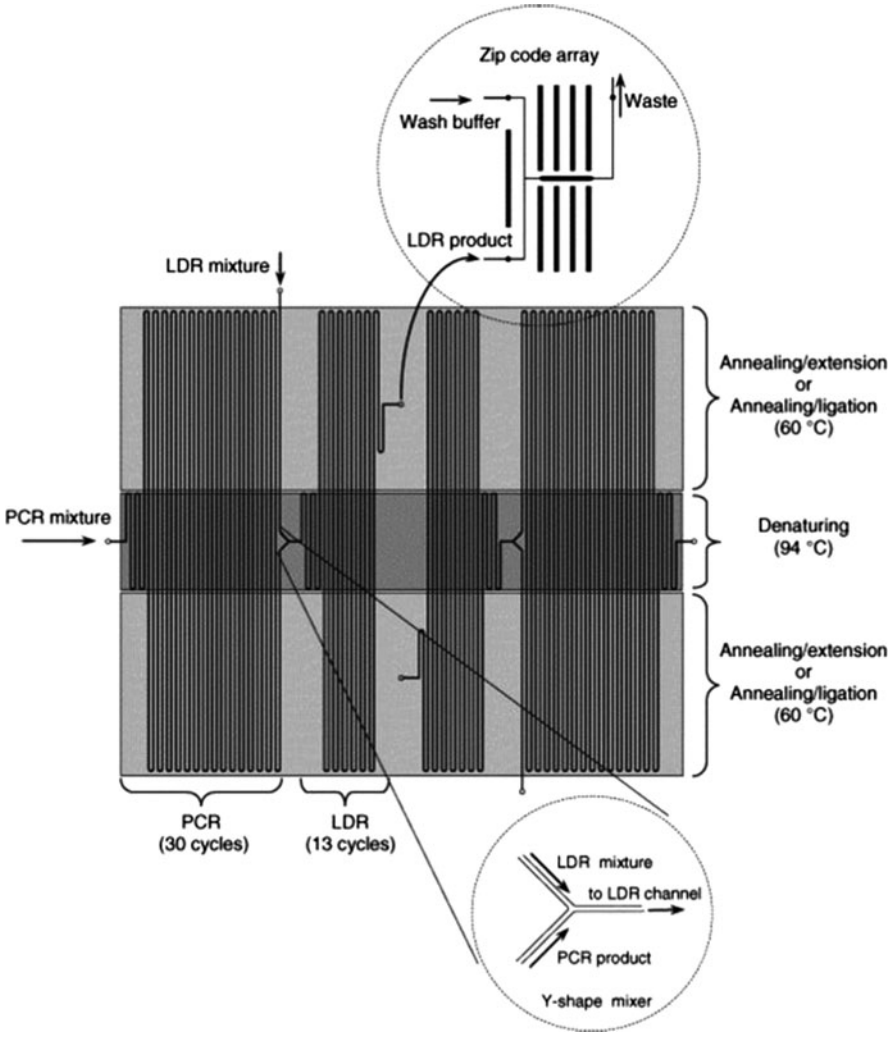

Fig. 15 Topographical layout of a CFPCR/CFLDR device. The microchip possessed channels that were 50 μm in width and 100 μm in depth with a 400 μm interchannel spacing. The total length of the thermal cycling channel was 2.28 m and consisted of a 30-cycle PCR (1.57 m long) and a 13-cycle LDR (0.71 m long). The *top inset* represents a microscope image of the turns of the CF thermal cycling channel. The *bottom inset* is an enlarged schematic of the Y-shaped passive micromixer for mixing the PCR product with the LDR cocktail. Three different Kapton film heaters were attached to the appropriate positions on the CFPCR/CFLDR chip for providing the required isothermal zones. Thermocouples were inserted between the microchip cover plate and the film heaters for monitoring the temperatures. Reproduced from [208] with permission

E. coli (a thiazole orange intercalating dye was admixed to label the PCR products for fluorescence detection). The thermal cycling device also used printed-ink contact resistors, which allowed heating at 12 °C/s. The system was used to identify

E. coli O157:H7 organisms. An LOD of ~6 copies of target DNA was reported using this system.

Easley et al. [10] developed a microfluidic genetic analysis (MGA) system fabricated on a glass substrate. The MGA was capable of accepting whole blood as a crude biological sample for the detection of *Bacillus anthracis* (anthrax) in 750 nL of whole blood from living asymptomatic infected mice, with the endpoint generation of a genetic profile. To demonstrated the sample-in-answer-out capability of the integrated monolithic chip (see Fig. 16), the blood was mixed with a lysis buffer and a volume equivalent to 750 nL (containing 15–45 ng of murine DNA) of whole blood was loaded onto the device with subsequent DNA extraction, a process which was completed in <10 min. DNA extractions used silica beads (5–30 μm) that were packed into the SPE domain (see Fig. 16d) against an etched weir filter by using an applied vacuum and replaced before each analysis. Flow rates employed for all extractions were 4.16 μL/min. Upon capture of the purified DNA in a 550-nL PCR microchamber, IR-mediated thermal cycling was performed to generate a 211-bp amplicon found on plasmid pX01 of *B. anthracis* (11 min processing time for the PCR). This was followed by pressure-injection of postamplified products into the separation domain of the chip along with a DNA sizing ladder and, then, electrokinetic injection into a separation channel for electrophoretic sorting, which was carried out in <180 s. The entire sample processing could be completed in <30 min (see Fig. 17).

Thaitrong et al. [252] fabricated a PCR-CE microsystem manufactured on a glass substrate, whose layout is shown in Fig. 18a. In this work, two types of injectors were compared: a sidearm injector (see Fig. 18b) that utilized a cross-T injection mode, and an in-line injector (see Fig. 18c) that employed a ~1-mm μCE section of crosslinked DNA affinity-capture matrix synthesized in situ by co-photopolymerizing acrylamide with 5′ acrydite-modified oligonucleotide capture probes [253]. For the in-line injector strategy, the PCR products were captured and preconcentrated before thermal release and injection. This strategy was demonstrated with PCR-μCE multiplexed analysis of *E. coli* K12 and *E. coli* O157:H7, where the in-line injector eliminated band broadening and increased the injection efficiency to ~100%. In addition, the on-chip generated PCR amplicons processed on this system with an oligonucleotide affinity capture gel exhibited ~3.6-fold increase in the signal-to-noise ratio, a sixfold increase in resolution, and yielded separation efficiencies in the range of 2×10^5 plates/m compared to the sidearm injector [254, 255].

There is need for portable field testing systems to perform DNA typing, microbial forensics, and ensure public health. For example, point-of-use systems are needed to determine the presence of microorganisms that are potentially harmful to humans [256]. These applications would benefit from a portable microsystem that could provide robust, quantitative analyses for the detection of infectious diseases or analyze DNA forensic samples in a timely manner.

Along these lines, Lagally and coworkers [111] reported an integrated portable genetic analysis microsystem to perform pathogen detection and genotyping directly from whole *E. coli* and *Staphylococcus aureus* cells. The system contained

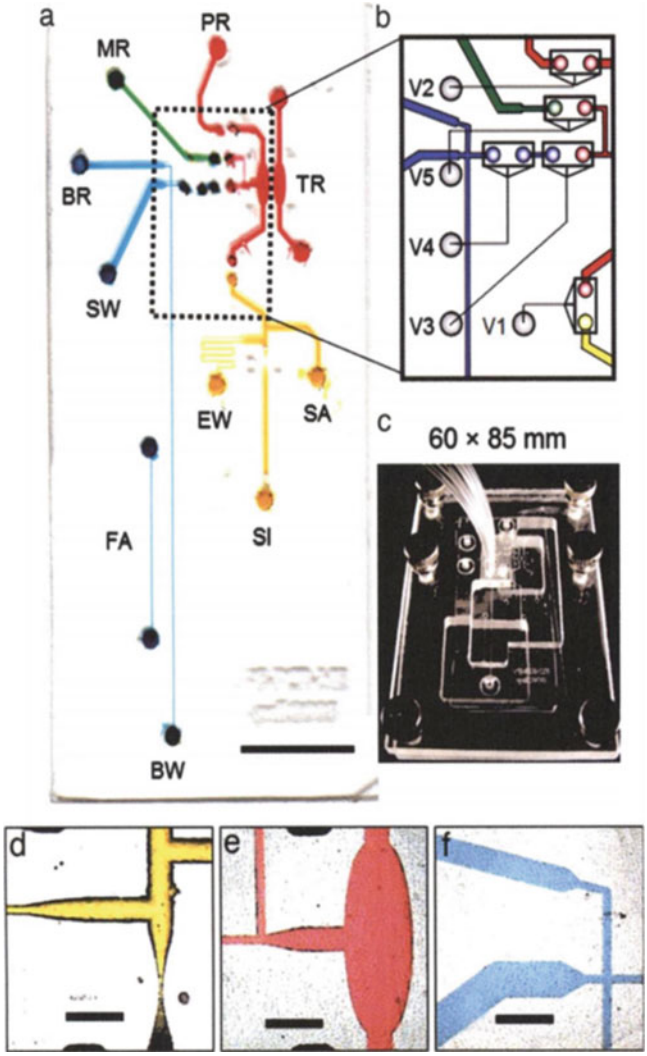

Fig. 16 Microfluidic genetic analysis (MGA) system. (**a**) Dyes are placed in the channels for visualization (*Scale bar*: 10 mm). Domains for DNA extraction (*yellow*), PCR amplification (*red*), injection (*green*), and separation (*blue*) are connected through a network of channels and vias. SPE reservoirs are labeled for sample inlet (*SI*), sidearm (*SA*), and extraction of waste (*EW*). Injection reservoirs are labeled for the PCR reservoir (*PR*), marker reservoir (*MR*), and sample waste (*SW*). Electrophoresis reservoirs are labeled for the buffer reservoir (*BR*) and buffer waste (*BW*). Additional domains patterned onto the device included the temperature reference (*TR*) chamber and fluorescence alignment (*FA*) channel. The flow control region is outlined by a *dashed box*. Device dimensions are 30.0 × 63.5 mm with a total solution volume <10 μL (*Scale bar*: 10 mm). (**b**) Flow control region. Valves are shown as *open rectangles*. *V1* separates the SPE and PCR domains. *V2* and *V5* are inlet valves for the pumping injection, *V3* is the diaphragm valve, and *V4* is an outlet valve. (**c**) Device loaded into the manifold. (**d**) Intersection between SI and SA inlet channels, with the EW channel tapering to increase flow resistance (*Scale bar*: 1 mm).

a single 200-nL PCR amplification chamber directly connected to a μCE separation microchannel, with turns to increase its length. The chip was coupled with a compact electrical control and laser-induced fluorescence (LIF) detector. The system contained microfabricated Ti/Pt heaters with gold leads on the reverse side of the chip, Ti/Pt resistance temperature detectors (RTDs) fabricated within the PCR chamber, and membrane valves to provide controlled sample positioning within the 200-nL PCR chamber (see Fig. 19). In this work, two novel PDMS microvalves were assembled on the top surface of the system. These microvalves exhibited dead volumes as low as 8 nL and were actuated with small pressures and vacuums [257]. Pt electrodes were also placed within the system, allowing application of high voltages without the need for external electrodes. The microsystem was the size of a microscope slide and was placed into a portable analysis instrument containing all of the necessary electronics, optics, and control hardware for conducting genetic analyses (form factor was 20.3 cm × 25.4 cm × 30.5 cm). This microsystem was used to perform a triplexed PCR targeting genes that encode for 16S ribosomal RNA, the flagellar antigen, and the shiga toxin in *E. coli*. Fluorescein-labeled PCR products were electrophoretically analyzed in $<$10 min.

A portable field testing system for performing human identification via DNA typing directly at a crime scene can be used to rapidly identify potential suspects. In the work of Liu et al. [5], a portable forensic genetic analysis system consisting of two identical PCR-CE systems symmetrically arranged on a 4″. wafer for the amplification and separation of short tandem repeats (STRs) was reported. The structure of the system was similar to that developed by Lagally et al. [111] (see Fig. 19), but the design was modified to accommodate field use. The fluidic chip consisted of a 160-nL PCR chamber, integrated Ti/Pt heaters with gold leads fabricated on the reverse side of the chip, a Ti/Pt four-point RTD fabricated within the PCR chamber, and a 7-cm μCE separation channel. The instrument integrated the following processing steps: PCR thermal cycling, electrophoretic separation, pneumatic valve fluidic control, and four-color laser-induced fluorescence detection. The multiplexing capability was demonstrated using a quadruplex Y-chromosome STR typing system consisting of the amelogenin gene and three Y STR loci (DYS390, DYS393, and DYS439). In this work, 35 PCR cycles for the amplification of all four loci, followed by CE separation and four-color fluorescence detection, was completed in 1.5 h. [10]. Liu and coworkers[258] also demonstrated the capabilities of this portable microsystem for crime scene investigation processes by performing real-time nine-plex autosomal STR analyses at a mock crime scene to secure male and female STR profiles (see Fig. 20) with 100-copy sensitivity. In this demonstration, all alleles were sized correctly in 2.5 h with a standard deviation $\leq$0.8 bp.

Fig. 16 (Continued) (**e**) PCR chamber with exit channel tapering before intersecting with the MR inlet channel (*Scale bar*: 1 mm). (**f**) Cross-T intersection (*Scale bar*: 1 mm). The relative sizes of the BR, SW, and BW channels create the difference in volume displacement during the pumping injection and affect how the resistance is dropped under an applied separation voltage. Reproduced from [10] with permission

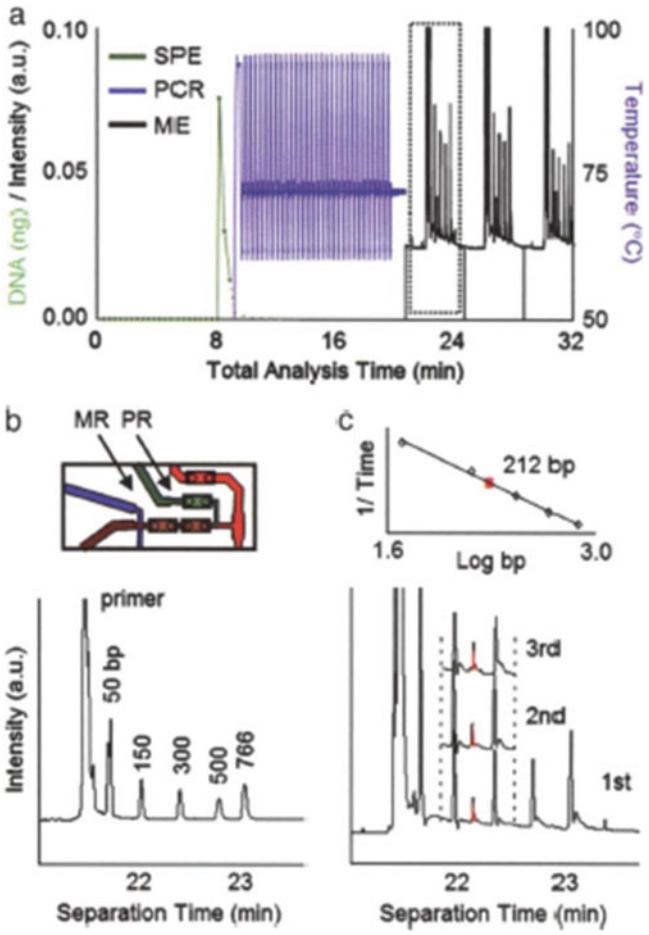

Fig. 17 Detection of *B. anthracis* from murine blood. (**a**) Detector responses during all three stages of sample processing and analysis are portrayed in terms of total analysis time. The SPE trace (*green*) was taken from off-line DNA extraction of the same murine sample and is representative of the total DNA concentration observed in a typical extraction. The temperature (*blue*) and fluorescence intensity (*black*) represent on-line data, with a total analysis time <24 min. Three sequential injections and separations were carried out to ensure the presence of amplified product. (**b**) Fluorescence data from an integrated analysis of a blank sample (no DNA) control with marker peaks labeled. The *inset* represents valve actuation during co-injection, with the PR and MR pumping inlets indicated by the *arrows*. (**c**) Zoomed view of the first separation shown in (**a**), with the product peak marked. The second and third runs are overlaid with the time axis cropped. *Inset* shows the sizing curve of inverse migration time vs. log(base pairs) with both the sizing standard peaks (*open diamonds*) and product (*square*) plotted for all three runs shown in (**a**). From these data, the product was 211 ± 2 bp. Reproduced from [10] with permission

Mathies and his group [54] reported a nanoliter-scale fluidic bioprocessor that integrated three processing steps of Sanger sequencing (thermal cycling, sample purification, and CE) into a single monolithic system. The fluidic system

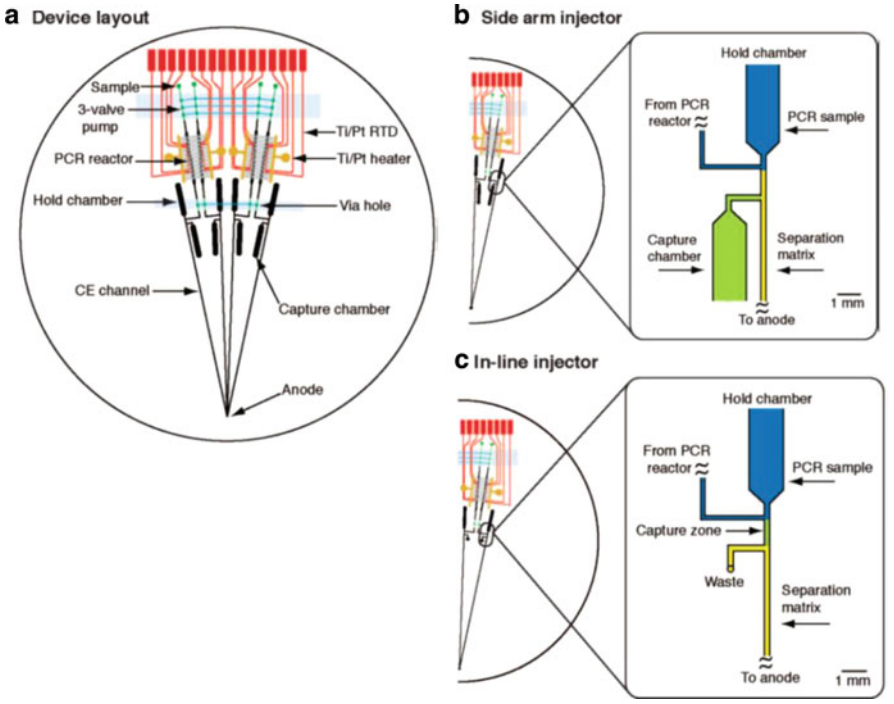

Fig. 18 (**a**) Layout of the PCR-CE microsystem with integrated sample cleanup. Each of the four analyzers is composed of a three-valve pump for fluidic control, an RTD temperature sensor and integrated heater for thermal cycling, a 250-nL PCR reaction chamber, etched chambers for analyte capture and purification, and μCE separation channels 5 cm in length. (**b**) Expanded view of the sidearm capture structure. A capture matrix made of 6.5% linear polyacrylamide (LPA) gel copolymerized with an oligonucleotide capture probe is manually loaded from the sidearm into the capture chamber. (**c**) Expanded view of the in-column capture structure. An in-situ photopolymerized capture matrix made of 5% acrylamide/bis gel copolymerized with an oligonucleotide capture probe is polymerized in a capture zone (40 mm deep × 120 mm wide × 1 mm long) directly in-line with the separation channel. Reproduced from [252] with permission

(see Fig. 21a) was microfabricated using a hybrid glass/PDMS wafer with the following three devices: (1) thermal cycling (TC) device, which consisted of a 250-nL reaction chamber with integrated resistive temperature probes, microvalves, and surface heaters; (2) affinity-capture purification chambers for cleaning up the reaction products prior to electrophoretic sorting; and (3) μCE channels 30 cm in length that was folded via turns 65 μm in width. The pneumatic valves and pumps were also included in the microsystem. Overall, the system was comprised of four-layers, three of which were glass wafers 100 mm in diameter that contained the fluidic channels and a final layer consisting of a PDMS membrane. The reaction chambers and μCE channels were etched between two thermally bonded glass wafers, while channel interconnections and microvalves were formed

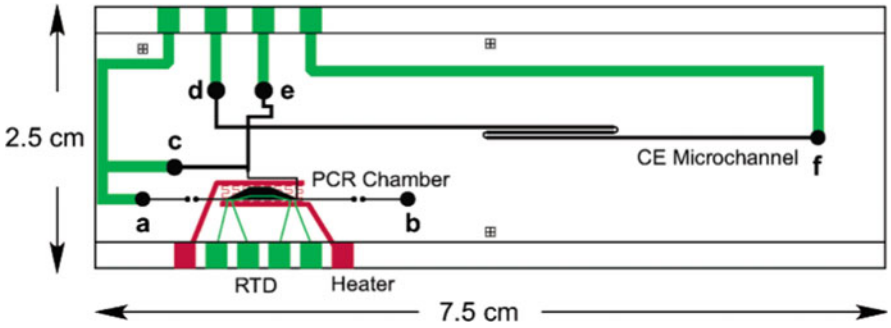

Fig. 19 Mask design for the portable PCR-CE system. The glass microchannels are indicated in *black*, the RTD and microfabricated electrodes are in *green*, and the heater (located on the back of the device) is shown in *red*. The PCR chamber is loaded through reservoirs *a* and *b*. Reservoir *c* is the co-inject reservoir, *d* is the cathode, *e* is the waste, and *f* is the anode. Reproduced from [111] with permission

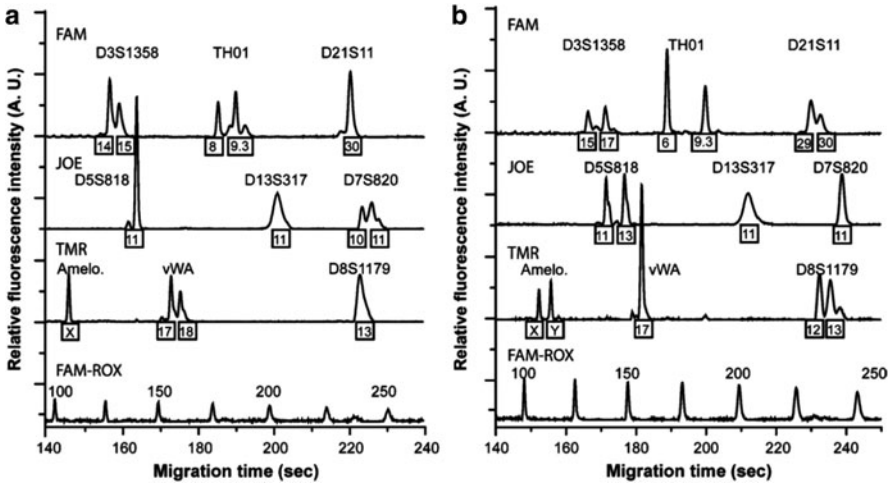

Fig. 20 Representative nine-plex STR profiles of (**a**) 9,947A female and (**b**) 9,948 male standard DNA obtained with 100 copies of DNA template in the PCR chamber of an integrated microfluidic system. Reproduced from [258] with permission

by the PDMS and a bottom manifold glass wafer. The system was demonstrated for complete Sanger sequencing from only 1 fmol of DNA template, with 556 continuous bases sequenced at 99% accuracy (see Fig. 21g), demonstrating read lengths appropriate for de novo sequencing of human and other complex genomes. The base-call accuracy estimates were accumulated using PHRED 0.020425.C. [259].

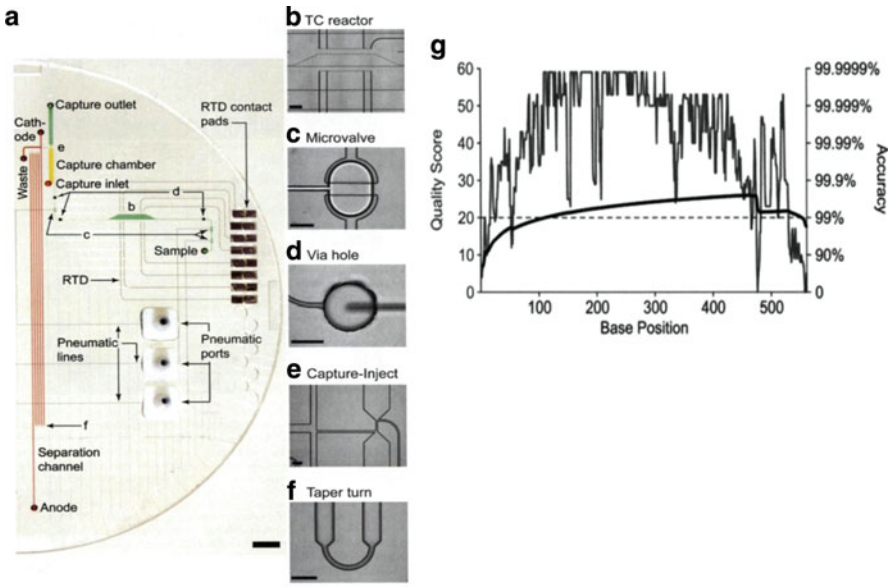

Fig. 21 (**a**) Photograph of the system bioprocessor components showing a DNA processing system. Colors indicate the location of sequencing reagent (*green*), capture gel (*yellow*), separation gel (*red*), and pneumatic channels (*blue*) (*Scale bar*: 5 mm). Component microphotographs b (*Scale bar*: 1 mm), c-f (*Scale bars*: 300 μm): (**b**) 250-nL thermal cycling reactor with RTDs; (**c**) 5-nL displacement volume microvalve; (**d**) via hole 500 g in diameter; (**e**) capture chamber and cross-injector; (**f**) taper 65 μm in width that folded the 30-cm channel to minimize turn-induced dispersion. (**g**) Base-call accuracies and sequence read length as predicted by PHRED. Percentage accuracy is related to the PHRED quality score by $100(1 - P_e)$, where P_e is the probability that the base call is incorrect and is equal to $1/10^{Q/10}$. A one-in-a-hundred error rate is indicated by the *dashed line*. PHRED quality scores are plotted at each base position. The *thick black line* charts predicted read accuracy at each base position: $100(\text{Base}_i - \Sigma\, Pe_i)/\text{Base}_i$, where Base_i is base position. Reproduced from [54] with permission

4.2 *Integrated Systems with Microarray Readout*

Unitizing the advantages of microchip-based DNA microarrays such as the highly parallel nature of the readout and the ability to screen DNA sequences with high specificity, numerous attempts have been made to incorporate front-end sample processing strategies with DNA microarrays used as the terminal readout step onto a single microfluidic platform. The front-end processing strategies that are needed prior to microarray readout are similar in nature to those required for μCE and are delineated in Fig. 1. The operational differences, in terms of microsystems using arrays versus μCE include:

1. No need for high voltage power supplies
2. Imaging over relatively larger areas when fluorescence detection is employed (imaging optics versus point detection of μCE)

3. On-chip heaters to control the temperature of the array, depending on the level of hybridization stringency required
4. Reduced processing times compared to μCE due to the small diffusional distances associated with microfluidics

Several examples of front-end process integration and microarrays to form functional microsystems have been reported in the literature [69, 78, 98, 114, 208, 210, 260–262].

One of the initial microsystems reported was by Anderson et al. [69] over a decade ago. A monolithic biochemical processing unit (BPU) was interfaced to a GeneChip commercialized by Affymetrix for performing multistep molecular processing of genomic samples and included extracting and concentrating of nucleic acids from a serum lysate, amplification (RT-PCR and nested PCR), enzymatic reactions (fragmentation, dephosphorylation, and labeling), metering, mixing, and hybridization to the GeneChip. The system was fabricated in PC using conventional computer-controlled micromachining. Temperatures were controlled by pressing thermal elements against the thin wall of the PC cartridge, with Peltier junctions used for heating and cooling. Fluidic manipulation was achieved through the use of a fluid barrier or hydrophobic membrane in conjunction with a pneumatically controlled diaphragm valve and hydrophobic vent. The system performance was evaluated using serum samples loaded with HIV virus. Analysis of the GeneChip results yielded an average accuracy of 99.7%, as determined by independent sequencing.

Liu et al. [98] presented a disposable, monolithic device that integrated PCR and a DNA microarray. The system was also fabricated in PC using CO_2 laser machining (see Fig. 22a). This system was assembled using a two-step process: First, thermal fusion bonding of PC was performed at 139 °C and under 2 tons of pressure for 45 min with a square window for the DNA array left open. Second, following surface activation and oligonucleotide probe immobilization using a Motorola proprietary attachment chemistry through the access window, the window was closed with another piece of properly sized PC using double-sided tape. The bonding was enforced by applying 2 tons of pressure for 2 min, and then the edges were sealed with epoxy. During PCR thermal cycling, the PCR device of the monolithic chip was sandwiched between two Peltier elements to allow thermal processing of the sample, with temperatures being monitored using thermocouples. Microfluidic control was accomplished through the use of three external syringe pumps docked to the system in combination with four on-chip Pluronics polymer valves and one hydrophobic valve. Asymmetrical PCR amplification and subsequent hybridization analysis of both *E. coli* and *Enterococcus faecalis* was demonstrated. However, the use of PC as the microarray platform generated a significant amount of autofluorescence, which degraded the detection limits for fluorescence readout (see Fig. 22b).

To overcome this problem, Hashimoto et al. [208] coupled CFPCR and continuous flow LDR (CFLDR) devices, both fabricated using a PC substrate, with a universal microarray fabricated using a PMMA substrate, which possesses better

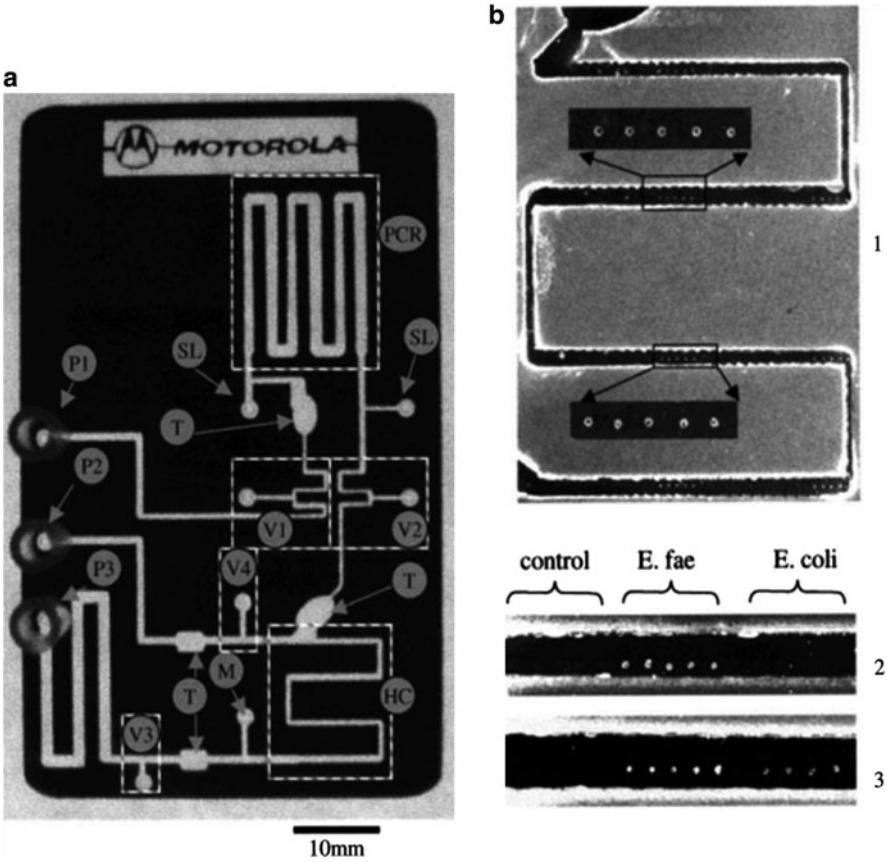

Fig. 22 (**a**) Monolithic integrated polycarbonate DNA analysis system. The system contained a serpentine PCR channel (*PCR*), a hybridization channel (*HC*), a syringe coupled to a hybridization wash solution channel, a waste channel coupled to a waste syringe, Pluronic traps (*T*), one hydrophobic air-permeable membrane valve (*M*), four Pluronics valves (*V1–V4*), two PCR reagent loading holes (*SL*), and three external syringe pumps interfaced to reservoirs: sample driving syringe pump (*P1*), waste-withdrawing syringe pump (*P2*), and wash syringe pump (*P3*). The dimensions of the system were 5.4 cm × 8.6 cm × 0.75 mm. (**b**) PCR hybridization results from the monolithic integrated system. *1 E. coli* 221-bp hybridization after amplification. Portions of the channel are enlarged for better viewing. *2* Fluorescent image of portion of the channel after *E. faecalis* amplification and hybridization. *3* Fluorescent image of portion of the channel after multiplex (*E. faecalis* and *E. coli*) amplification and hybridization. Reproduced from [98] with permission

optical properties with lower autofluorescence levels compared to PC (see Fig. 15). The chip was generated via microreplication (hot embossing) from metal molding tools fabricated using high-precision micromilling. The CFPCR/CFLDR chip was directly attached to thin film heaters for providing the set temperatures for the isothermal zones, with thermocouples embedded between the cover plate and the film heaters for monitoring the set temperatures required for both PCR and LDR.

In this work, low density universal microarrays were produced on the bottom floor of a UV-photoactivated PMMA microchannel, with the DNA zipcode probes attached to UV-generated carboxylic acid groups. PCR amplicons were used as templates for the allele-specific CFLDR, which produced single-stranded targets that were uniformly flowed over the universal array to reduce incubation times. Using a mixed population of genomic DNA as starting materials, one mutant in 80 wild-type sequences could be successfully discriminated in a total reaction time of 50 min, including 18.7 min for PCR, 8.1 min for LDR, 5 min for hybridization, 10 min for washing, and 2.6 min for fluorescence imaging of the low-density array. The authors also showed the ability to reduce reagent consumption by one order of magnitude compared to similar benchtop assays.

A self-contained biochip that integrated cell isolation and lysis with PCR amplification and electrochemical microarray-based detection was described by Liu et al. [262] The chip was machined in a PC substrate using a conventional computer-controlled milling machine and included a mixing unit for cell capture using immunomagnetic beads, a cell preconcentration/purification/lysis/PCR unit, and a DNA microarray chamber. In this work, fluidic components (e.g., paraffin-based microvalves, cavitation microstreaming mixers, and electrochemical or thermopneumatic pumps), embedded resistive heaters, and DNA microarray sensors were coupled to the system to perform DNA analysis of biological samples. Electrical power, PCR thermal cycling, DNA electrochemical signal readout, and magnetic elements for bead arrest were controlled by an off-chip instrument. Implementation of cavitation microstreaming has been shown to achieve cell capture efficiencies on the order of 73% using immunomagnetic beads and up to a fivefold reduction in hybridization time compared to passive incubation of the array with solution targets, as well as improved signal uniformity. Detection of pathogenic *E. coli* K12 cells seeded into rabbit blood and single-nucleotide polymorphism analysis from diluted blood samples were completed in 3.5 and 2.7 h, respectively.

Soper et al. [210] designed a polymer-based modular microsystem that could accept a crude sample and automatically carry out the entire molecular processing pipeline in an enclosed fluidic cartridge (see Fig. 23). The multistep assay included bacterial cell lysis, SPE of genomic DNA from the lysate, PCR amplification, LDR, and universal DNA array readout. The fluidic cartridge was generated via microreplication from the appropriate metal molding tools, which were used to create structures on both sides of the polymer substrate (i.e., double-sided hot embossing). The integrated fluidic cartridge was comprised of a fluidic motherboard and two modules. One module was made from PC and used for SPE, while the other module was made from PMMA and contained DNA probes patterned on a planar waveguide for evanescent excitation. These modules were interconnected to a fluidic motherboard fabricated in PC and were used for processing steps for thermal cell lysis, PCR, and LDR. Fluid handling, thermal management, and optical detection were controlled by off-chip supporting peripherals, which could be packaged into a small footprint instrument (1 ft^3). Identification of multidrug-resistant tuberculosis (MDR-TB) resulting from *Mycobacterium tuberculosis* (Mtb) strains in clinical sputum samples were demonstrated with a detection limit of ~50 bacterial cells

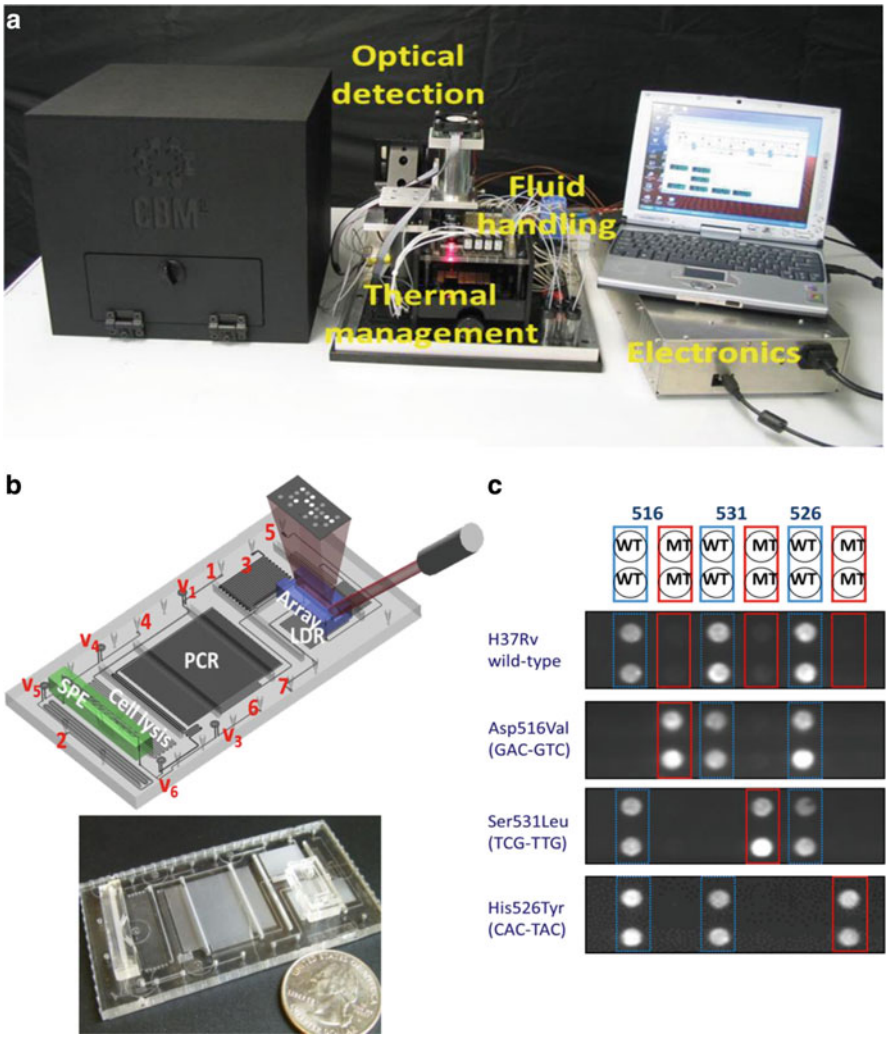

Fig. 23 Integrated, modular microfluidic chip for TB analysis. (**a**) Overview of the integrated system. The system had dimensions 12″ (length) × 12″ (width) × 12″ (height), and all fluid handling, thermal management, and optical detection were controlled by off-chip supporting peripherals and assembled into a small form factor instrument. (**b**) Schematic and photograph of the fluidic cartridge. The fluidic cartridge was composed of two modules and a fluidic motherboard. The fluidic motherboard was made from PC and consisted of processing steps for cell lysis, PCR, and LDR. One module was made from PC and used for SPE of genomic DNA, while the other module was made from PMMA and contained an air-embedded planar waveguide and the DNA array. Sample inlet (*1*), PCR mixture inlet (*2*), LDR mixture inlet (*3*), ethanol and air inlet (*4*), array wash inlet (*5*), vacuum connection (*6*), and waste outlet (*7*). *V1–V6* were on-chip membrane valves. *V2* is positioned next to the SPE module on the cell lysis microchannel and is not visible in current view. (**c**) Molecular assay results from drug-susceptible *Mycobacterium tuberculosis* (Mtb) strains and drug resistant Mtb strains. *516WT*, *531WT* and *526WT* are probes targeting drug-susceptible Mtb strains. *516MT*, *531MT*, and *526MT* are probes targeting drug-resistant Mtb strains. Reproduced from [210] with permission

from sputum (processing time <40 min). In addition to MDR-TB detection, the modular fluidic cartridge could be reconfigured for use with other assay formats, such as PCR-μCE.

5 Concluding Remarks

There have been extensive reports on devices designed to perform a single-step in the analysis of a variety of nucleic acids, such as DNAs and RNAs. These devices have been fabricated using a variety of micromanufacturing techniques in different substrate materials. Devices have been developed for the SPE of nucleic acids from clinical, environmental, or crime-scene samples employing beads, polymer monoliths, or fabricated pillars to produce the desired solid phase. In addition, a plethora of devices focused on thermal cycling (such as that required for PCR, cycle sequencing, or allele-specific LDR) have been detailed in the literature and typically use either a chamber-type approach, in which the chamber and its contents are cycled between the desired temperatures, or a continuous flow operation, in which isothermal zones are situated on the chip and the reaction fluid is transported through these isothermal zones. Devices have also been reported that perform μCE separation of DNAs using sieving matrices with various channel lengths to reach the desired resolution demanded of the separation. While these represent innovative concepts, the complete analysis of different sample types required for genetic analyses typically requires a number of processing steps (see Fig. 1). Therefore, it is clear that integration of many of the aforementioned devices to form functional and autonomously operated systems needs to be undertaken. However, process integration to form autonomous systems is not simply a matter of "hooking" together the various devices outlined previously. For example, many of the upstream processing steps and the reagents they require may be detrimental to those poised downstream. Also, some steps demand hydrodynamically driven flow, while others require electrokinetically driven flow. Another concern is unswept volumes, which can generate sample carryover artifacts or sample loss, especially when dealing with ultrasmall sample volumes. Some substrate materials do not accommodate particular processing steps, and high optical quality materials must be used for assays employing fluorescence as the detection mode. Finally, some process steps require thermal control, such as PCR, and these thermally actuated units must be isolated from those that are sensitive to temperature, such as microarrays.

Several examples of integrated microfluidic systems have been presented herein, most of which are proof-of-concept demonstrations with only a few examples that have actually dealt with clinical or "real-world" samples. Unfortunately, many of these demonstrators of integrated microfluidic systems, while attractive in terms of their ability to reduce sample processing time and reagent consumption, have only been utilized in research settings. Some of the more compelling applications for integrated microfluidic systems, such as in vitro diagnostics, homeland security, or forensics, will demand systems that can accommodate field analysis and/or one-time

use operation. For example, in the case of in vitro diagnostics, it will be necessary to use the entire microfluidic system for a single patient sample, demanding that the cost of the chip be low. In addition, field analysis applications will require not only that the chip possesses a small footprint, but also that the support peripherals must have the same characteristic. These support peripherals include pumps, valves, reagent reservoirs, electronics, and optomechanics if some type of optical readout is used. The chip and support peripherals must all be packaged into a small form factor instrument and must consume minimal amounts of power to enable battery operation for extended periods of time. All this must be engineered without sacrificing assay performance in terms of reproducibility, LOD, sensitivity, and specificity.

Another interesting aspect is related to the manufacturability of the system. For wide spread commercialization, the fluidic system must be produced in high volume and at low cost. Chip production not only includes the microfabrication of the channel networks, but also chip assembly, integration of various components such as electrodes, optical elements, and valves and, finally, the surface attachment of necessary biologics to effect the desired process step. Although microfluidics has shifted from the use of silicon, glass, and other similar materials that require extensive microfabrication procedures to the use of polymer substrates that can use microreplication processes (similar to those used to produce CDs and DVDs) to produce the desired fluidic networks in a high production mode with good fidelity, the challenge still remains in chip finishing following production of the fluidic network.

The driving force behind the increasing development of integrated microfluidic systems is certainly due to their potential commercialization, but also in their diverse applications in such areas as biology, chemistry, and other disciplines that strongly demand the emergence of new analysis platforms to achieve higher performance and throughput. Because direct integration of PCR with other sample preparation protocols, including μCE, fluorescence, and microarrays has been demonstrated for a wide range of applications (pathogen detection, DNA typing, and DNA sequencing), these success stories will demand higher functionality at lower cost and with higher throughput. Such systems offer compelling advantages such as short assay turnaround times, automated operation, improved operator protection, lower cross-contamination, reduced human error, and lower overall assay cost. Minimization of potential carryover contamination from run-to-run is a key consideration in providing accurate and reliable results and the use of disposable fluidic cartridges will effectively minimize this risk.

References

1. Collins FS, Morgan M, Patrinos A (2003) Science 300:286
2. Aboud MJ, Gassmann M, McCord BR (2010) Electrophoresis 31:2672
3. Hopwood AJ, Hurth C, Yang J, Cai Z, Moran N, Lee-Edghill JG, Nordquist A, Lenigk R, Estes MD, Haley JP, McAlister CR, Chen X, Brooks C, Smith S, Elliott K, Koumi P, Zenhausern F, Tully G (2010) Anal Chem 82:6991

4. Horsman KM, Bienvenue JM, Blasier KR, Landers JP (2007) J Forensic Sci 52:784
5. Liu P, Seo TS, Beyor N, Shin KJ, Scherer JR, Mathies RA (2007) Anal Chem 79:1881
6. Chovan T, Guttman A (2002) Trends Biotechnol 20:116
7. Verpoorte E (2002) Electrophoresis 23:677
8. Khandurina J, McKnight TE, Jacobson SC, Waters LC, Foote RS, Ramsey JM (2000) Anal Chem 72:2995
9. Koh CG, Tan W, Zhao MQ, Ricco AJ, Fan ZH (2003) Anal Chem 75:4591
10. Easley CJ, Karlinsey JM, Bienvenue JM, Legendre LA, Roper MG, Feldman SH, Hughes MA, Hewlett EL, Merkel TJ, Ferrance JP, Landers JP (2006) Proc Natl Acad Sci USA 103:19272
11. Pal R, Yang M, Lin R, Johnson BN, Srivastava N, Razzacki SZ, Chomistek KJ, Heldsinger DC, Haque RM, Ugaz VM, Thwar PK, Chen Z, Alfano K, Yim MB, Krishnan M, Fuller AO, Larson RG, Burke DT, Burns MA (2005) Lab Chip 5:1024
12. deMello AJ (2006) Nature 442:394
13. Beebe DJ, Mensing GA, Walker GM (2002) Annu Rev Biomed Eng 4:261
14. Manz A, Graber N, Widmer HM (1990) Sens Actuators B Chem 1:244
15. Kan CW, Fredlake CP, Doherty EAS, Barron AE (2004) Electrophoresis 25:3564
16. Woolley AT, Mathies RA (1995) Anal Chem 67:3676
17. Schmalzing D, Adourian A, Koutny L, Ziaugra L, Matsudaira P, Ehrlich D (1998) Anal Chem 70:2303
18. Di Carlo D, Ionescu-Zanetti C, Zhang Y, Hung P, Lee LP (2005) Lab Chip 5:171
19. Irimia D, Tompkins RG, Toner M (2004) Anal Chem 76:6137
20. Waters LC, Jacobson SC, Kroutchinina N, Khandurina J, Foote RS, Ramsey JM (1998) Anal Chem 70:158
21. Belgrader P, Hansford D, Kovacs GTA, Venkateswaran K, Mariella R, Milanovich F, Nasarabadi S, Okuzumi M, Pourahmadi F, Northrup MA (1999) Anal Chem 71:4232
22. Taylor MT, Belgrader P, Furman BJ, Pourahmadi F, Kovacs GTA, Northrup MA (2001) Anal Chem 73:492
23. Lu H, Schmidt MA, Jensen KF (2005) Lab Chip 5:23
24. Lee SW, Tai YC (1999) Sens Actuators A Phys 73:74
25. Wang HY, Bhunia AK, Lu C (2006) Biosens Bioelectron 22:582
26. Nevill JT, Cooper R, Dueck M, Breslauer DN, Lee LP (2007) Lab Chip 7:1689
27. Abolmaaty A, El-Shemy MG, Khallaf MF, Levin RE (1998) J Microbiol Methods 34:133
28. Belgrader P, Benett W, Hadley D, Richards J, Stratton P, Mariella R, Milanovich F (1999) Science 284:449
29. Yang JM, Bell J, Huang Y, Tirado M, Thomas D, Forster AH, Haigis RW, Swanson PD, Wallace RB, Martinsons B, Krihak M (2002) Biosens Bioelectron 17:605
30. Fox MB, Esveld DC, Valero A, Luttge R, Mastwijk HC, Bartels PV, van den Berg A, Boom RM (2006) Anal Bioanal Chem 385:474
31. Wolfe KA, Breadmore MC, Ferrance JP, Power ME, Conroy JF, Norris PM, Landers JP (2002) Electrophoresis 23:727
32. Tian HJ, Huhmer AFR, Landers JP (2000) Anal Biochem 283:175
33. Breadmore MC, Wolfe KA, Arcibal IG, Leung WK, Dickson D, Giordano BC, Power ME, Ferrance JP, Feldman SH, Norris PM, Landers JP (2003) Anal Chem 75:1880
34. Legendre LA, Bienvenue JM, Roper MG, Ferrance JP, Landers JP (2006) Anal Chem 78:1444
35. Wu QR, Bienvenue JM, Hassan BJ, Kwok YC, Giordano BC, Norris PM, Landers JP, Ferrance JP (2006) Anal Chem 78:5704
36. Wen J, Guillo C, Ferrance JP, Landers JP (2007) Anal Chem 79:6135
37. Bhattacharyya A, Klapperich CM (2006) Anal Chem 78:788
38. Mahalanabis M, Al-Muayad H, Kulinski MD, Altman D, Klapperich CM (2009) Lab Chip 9:2811

39. Kulinski MD, Mahalanabis M, Gillers S, Zhang JY, Singh S, Klapperich CM (2009) Biomed Microdevices 11:671
40. Sauer-Budge AF, Mirer P, Chatterjee A, Klapperich CM, Chargin D, Sharon A (2009) Lab Chip 9:2803
41. Chung YC, Jan MS, Lin YC, Lin JH, Cheng WC, Fan CY (2004) Lab Chip 4:141
42. Wen J, Guillo C, Ferrance JP, Landers JP (2006) Anal Chem 78:1673
43. Legendre LA, Morris CJ, Bienvenue JM, Barron A, McClure R, Landers JP (2008) J Assoc Lab Auto 13:351
44. Christel LA, Petersen K, McMillan W, Northrup MA (1999) J Biomech Eng Trans ASME 121:22
45. Cady NC, Stelick S, Batt CA (2003) Biosens Bioelectron 19:59
46. Witek MA, Llopis SD, Wheatley A, McCarley RL, Soper SA (2006) Nucleic Acids Res 34:9
47. Witek MA, Hupert ML, Park DSW, Fears K, Murphy MC, Soper SA (2008) Anal Chem 80:3483
48. Park DSW, Hupert ML, Witek MA, You BH, Datta P, Guy J, Lee JB, Soper SA, Nikitopoulos DE, Murphy MC (2008) Biomed Microdevices 10:21
49. Kim J, Gale BK (2008) Lab Chip 8:1516
50. Kim J, Mauk M, Chen DF, Qiu XB, Gale B, Bau HH (2010) Analyst 135:2408
51. Xu YC, Vaidya B, Patel AB, Ford SM, McCarley RL, Soper SA (2003) Anal Chem 75:2975
52. Wang H, Chen JF, Zhu L, Shadpour H, Hupert ML, Soper SA (2006) Anal Chem 78:6223
53. Paegel BM, Yeung SHI, Mathies RA (2002) Anal Chem 74:5092
54. Blazej RG, Kumaresan P, Mathies RA (2006) Proc Natl Acad Sci USA 103:7240
55. Oleschuk RD, Shultz-Lockyear LL, Ning YB, Harrison DJ (2000) Anal Chem 72:585
56. Nakagawa T, Tanaka T, Niwa D, Osaka T, Takeyama H, Matsunaga T (2005) J Biotechnol 116:105
57. Cao WD, Easley CJ, Ferrance JP, Landers JP (2006) Anal Chem 78:7222
58. Saiki RK, Bugawan TL, Horn GT, Mullis KB, Erlich HA (1986) Nature 324:163
59. DeMello AJ (2003) Nature 422:28
60. Higuchi R, Fockler C, Dollinger G, Watson R (1993) Biotechnology 11:1026
61. Wiesner RJ (1992) Nucleic Acids Res 20:5863
62. Schönbrunner NJ, Fiss EH, Budker O, Stoffel S, Sigua CL, Gelfand DH, Myers TW (2006) Biochemistry 45:12786
63. Innis MA, Myambo KB, Gelfand DH, Brow MAD (1988) Proc Natl Acad Sci USA 85:9436
64. Northrup MA, Ching MT, White RM, Watson RT (1993) DNA amplification in a microfabricated reaction chamber. In: Proceedings seventh international conference on solid state sensors and actuators, Transducers'93, Yokohama, Japan, 7–10 June 1993, pp 924
65. Wilding P, Pfahler J, Bau HH, Zemel JN, Kricka LJ (1994) Clin Chem 40:43
66. Wilding P, Shoffner MA, Kricka LJ (1994) Clin Chem 40:1815
67. Wilding P, Shoffner MA, Cheng J, Hvichia G, Kricka LJ (1995) Clin Chem 41:1367
68. Soper SA, Ford SM, Xu YC, Qi SZ, McWhorter S, Lassiter S, Patterson D, Bruch RC (1999) J Chromatogr A 853:107
69. Anderson RC, Su X, Bogdan GJ, Fenton J (2000) Nucleic Acids Res 28:E60
70. Burns MA, Mastrangelo CH, Sammarco TS, Man FP, Webster JR, Johnson BN, Foerster B, Jones D, Fields Y, Kaiser AR, Burke DT (1996) Proc Natl Acad Sci USA 93:5556
71. Huhmer AFR, Landers JP (2000) Anal Chem 72:5507
72. Ferrance JP, Wu QR, Giordano B, Hernandez C, Kwok Y, Snow K, Thibodeau S, Landers JP (2003) Anal Chim Acta 500:223
73. Giordano BC, Ferrance J, Swedberg S, Huhmer AFR, Landers JP (2001) Anal Biochem 291:124
74. Giordano BC, Copeland ER, Landers JP (2001) Electrophoresis 22:334
75. Wilding P, Kricka LJ, Cheng J, Hvichia G, Shoffner MA, Fortina P (1998) Anal Biochem 257:95
76. Zhao Z, Cui Z, Cui DF, Xia SH (2003) Sens Actuators A Phys 108:162

77. Woolley AT, Hadley D, Landre P, deMello AJ, Mathies RA, Northrup MA (1996) Anal Chem 68:4081
78. Trau D, Lee TMH, Lao AIK, Lenigk R, Hsing IM, Ip NY, Carles MC, Sucher NJ (2002) Anal Chem 74:3168
79. Lagally ET, Emrich CA, Mathies RA (2001) Lab Chip 1:102
80. Liu J, Hansen C, Quake SR (2003) Anal Chem 75:4718
81. Zou QB, Miao YB, Chen Y, Sridhar U, Chong CS, Chai TC, Tie Y, Teh CHL, Lim TM, Heng C (2002) Sens Actuators A Phys 102:114
82. Zou QB, Sridhar U, Chen Y, Singh J (2003) IEEE Sens J 3:774
83. Dunn WC, Jacobson SC, Waters LC, Kroutchinina N, Khandurina J, Foote RS, Justice MJ, Stubbs LJ, Ramsey JM (2000) Anal Biochem 27:157
84. Matsubara Y, Kerman K, Kobayashi M, Yamamura S, Morita Y, Tamiya E (2005) Biosens Bioelectron 20:1482
85. Koh CG, Tan W, Zhao MQ, Ricco AJ, Fan ZH (2003) Anal Chem 75:6379
86. Easley CJ, Karlinsey JM, Landers JP (2006) Lab Chip 6:601
87. Kopp MU, de Mello AJ, Manz A (1998) Science 280:1046
88. Chiem N, Harrison DJ (1997) Anal Chem 69:373
89. Hashimoto M, Chen PC, Mitchell MW, Nikitopoulos DE, Soper SA, Murphy MC (2004) Lab Chip 4:638
90. Chen PC, Nikitopoulos DE, Soper SA, Murphy MC (2008) Biomed Microdevices 10:141
91. Chen PC, Park DS, You BH, Kim N, Park T, Soper SA, Nikitopoulos DE, Murphy MC (2010) Sens Actuators B Chem 149:291
92. Park DSW, Chen PC, You BH, Kim N, Park T, Lee TY, Datta P, Desta Y, Soper SA, Nikitopoulos DE, Murphy MC (2010) J Micromech Microeng 20:085011
93. Park DS, Wang H, Chen P-C, Park T, Kim N, You BH, Nikitopoulos DE, Soper SA, Murphy MC (2010) Passive micro-assembly of a fluidic control chip and a multi-well continuous flow PCR chip for high throughput applications. In: Proceedings 14th international conference on miniaturized systems for chemistry and life sciences, μTas2010, 3–7 October 2010, Groningen, Netherlands, pp 1126
94. Yeung SHI, Liu P, Del Bueno N, Greenspoon SA, Mathies RA (2009) Anal Chem 81:210
95. West J, Karamata B, Lillis B, Gleeson JP, Alderman J, Collins JK, Lane W, Mathewson A, Berney H (2002) Lab Chip 2:224
96. Roper MG, Easley CJ, Landers JP (2005) Anal Chem 77:3887
97. Chen JF, Wabuyele M, Chen HW, Patterson D, Hupert M, Shadpour H, Nikitopoulos D, Soper SA (2005) Anal Chem 77:658
98. Liu YJ, Rauch CB, Stevens RL, Lenigk R, Yang J, Rhine DB, Grodzinski P (2002) Anal Chem 74:3063
99. Curcio M, Roeraade J (2002) Anal Chem 75:1
100. Park N, Kim S, Hahn JH (2003) Anal Chem 75:6029
101. Liu J, Enzelberger M, Quake S (2002) Electrophoresis 23:1531
102. Sadler DJ, Changrani R, Roberts P, Chou CF, Zenhausern F (2003) IEEE Trans Compon Pack Technol 26:309
103. Chow AW (2002) AlChE J 48:1590
104. Zheng W, Chen S (2001) Proc SPIE 4560:256
105. Schneegass I, Kohler JM (2001) J Biotechnol 82:101
106. Hupert ML, Witek MA, Wang Y, Mitchell MW, Liu X, Bejat Y, Nikitopoulos DE, Goettert J, Murphy MC, Soper SA (2003) Proc SPIE 4982:52
107. Mitchell MW, Liu X, Bejat Y, Nikitopoulos DE, Soper SA, Murphy MC (2003) Proc SPIE 4982:83
108. Chen Z, Qian S, Abrams WR, Malamud D, Bau HH (2004) Anal Chem 76:3707
109. Zhang CS, Xu JL, Ma WL, Zheng WL (2006) Biotechnol Adv 24:243
110. Bu MQ, Melvin T, Ensell G, Wilkinson JS, Evans AGR (2003) J Micromech Microeng 13: S125

111. Lagally ET, Scherer JR, Blazej RG, Toriello NM, Diep BA, Ramchandani M, Sensabaugh GF, Riley LW, Mathies RA (2004) Anal Chem 76:3162
112. Lee DS, Park SH, Yang HS, Chung KH, Yoon TH, Kim SJ, Kim K, Kim YT (2004) Lab Chip 4:401
113. Lee DS, Wu MH, Ramesh U, Lin CW, Lee TM, Chen PH (2004) Sens Actuators B Chem 100:401
114. Lee TMH, Carles MC, Hsing IM (2003) Lab Chip 3:100
115. Rodriguez I, Lesaicherre M, Tie Y, Zou QB, Yu C, Singh J, Meng LT, Uppili S, Li SFY, Gopalakrishnakone P, Selvanayagam ZE (2003) Electrophoresis 24:172
116. Chou CF, Changrani R, Roberts P, Sadler D, Burdon J, Zenhausern F, Lin S, Mulholland A, Swami N, Terbrueggen R (2002) Microelectron Eng 61–2:921
117. Poser S, Schulz T, Dillner U, Baier V, Kohler JM, Schimkat D, Mayer G, Siebert A (1997) Sens Actuators A Phys 62:672
118. Belgrader P, Young S, Yuan B, Primeau M, Christel LA, Pourahmadi F, Northrup MA (2001) Anal Chem 73:286
119. Sun K, Yamaguchi A, Ishida Y, Matsuo S, Misawa H (2002) Sens Actuators B Chem 84:283
120. Fukuba T, Yamamoto T, Naganuma T, Fujii T (2004) Chem Eng J 101:151
121. Friedman NA, Meldrum DR (1998) Anal Chem 70:2997
122. Yang H, Choi CA, Chung KH, Jun CH, Kim YT (2004) Anal Chem 76:1537
123. Bruckner-Lea CJ, Tsukuda T, Dockendorff B, Follansbee JC, Kingsley MT, Ocampo C, Stults JR, Chandler DP (2002) Anal Chim Acta 469:129
124. Cady NC, Stelick S, Kunnavakkam MV, Batt CA (2005) Sens Actuators B Chem 107:332
125. Chaudhari AM, Woudenberg TM, Albin M, Goodson KE (1998) J Microelectromech Syst 7:345
126. Erill I, Campoy S, Rus J, Fonseca L, Ivorra A, Navarro Z, Plaza JA, Aguilo J, Barbe J (2004) J Micromech Microeng 14:1558
127. Grodzinski P, Liu RH, Chen B, Blackwell J, Liu Y, Rhine D, Smekal T, Ganser D, Romero C, Yu H, Chan T, Kroutchinina N (2001) Biomed Microdevices 3:275
128. Obeid PJ, Christopoulos TK, Crabtree HJ, Backhouse CJ (2003) Anal Chem 75:288
129. Zhou X, Liu D, Zhong R, Dai Z, Wu D, Wang H, Du Y, Xia Z, Zhang L, Mei X, Lin B (2004) Electrophoresis 25:3032
130. Gulliksen A, Solli L, Karlsen F, Rogne H, Hovig E, Nordstrøm T, Sirevåg R (2003) Anal Chem 76:9
131. Sethu P, Mastrangelo CH (2004) Sens Actuators B Chem 98:337
132. Shen K, Chen X, Guo M, Cheng J (2005) Sens Actuators B Chem 105:251
133. Slyadnev MN, Tanaka Y, Tokeshi M, Kitamori T (2001) Anal Chem 73:4037
134. Oda RP, Strausbauch MA, Huhmer AFR, Borson N, Jurrens SR, Craighead J, Wettstein PJ, Eckloff B, Kline B, Landers JP (1998) Anal Chem 70:4361
135. Wittwer CT, Fillmore GC, Hillyard DR (1989) Nucleic Acids Res 17:4353
136. Wittwer CT, Fillmore GC, Garling DJ (1990) Anal Biochem 186:328
137. Soper SA, Ford SM, Xu Y, Qi S, McWhorter S, Lassiter S, Patterson D, Bruch RC (1999) Proc SPIE 3602:392
138. Swerdlow H, Jones BJ, Wittwer CT (1997) Anal Chem 69:848
139. Wang Q, Gong H (2003) Proc SPIE 5119:77
140. Tanaka Y, Slyadnev MN, Hibara A, Tokeshi M, Kitamori T (2000) J Chromatogr A 894:45
141. Fermér C, Nilsson P, Larhed M (2003) Eur J Pharm Sci 18:129
142. Orrling K, Nilsson P, Gullberg M, Larhed M (2004) Chem Commun (7):790
143. Dietrich J, Schmitt P, Zieger M, Preve B, Rolland J-L, Chaabihi H, Gueguen Y (2002) FEMS Microbiol Lett 217:89
144. Ke C, Berney H, Mathewson A, Sheehan MM (2004) Sens Actuators B Chem 102:308
145. Pal D, Venkataraman V (2002) Sens Actuators A phys 102:151
146. Krishnan M, Ugaz VM, Burns MA (2002) Science 298:793
147. Chandrasekhar S (1961) Hydrodynamic and hydromagnetic stability. Clarendon, Oxford

148. Issaq HJ, Janini GM, Atamna IZ, Muschik GM (1991) J Liq Chromatogr 14:817
149. Jorgenson JW, Lukacs KD (1983) Science 222:266
150. Jorgenson JW, Lukacs KD (1981) Anal Chem 53:1298
151. Issaq HJ, Xu H, Chan KC (2001) J Liq Chromatogr Relat Technol 24:2381
152. Harrison DJ, Fluri K, Seiler K, Fan ZH, Effenhauser CS, Manz A (1993) Science 261:895
153. Woolley AT, Mathies RA (1994) Proc Natl Acad Sci USA 91:11348
154. Landers JP (1995) Clin Chem 41:495
155. Giddings JC (1969) Separ Sci 4:181
156. Boček P, Vespalec R, Giese RW (2000) Anal Chem 72:586A
157. Luckey JA, Norris TB, Smith LM (1993) J Phys Chem 97:3067
158. Lagally ET, Mathies RA (2004) J Phys D Appl Phys 37:R245
159. Meagher RJ, Won JI, McCormick LC, Nedelcu S, Bertrand MM, Bertram JL, Drouin G, Barron AE, Slater GW (2005) Electrophoresis 26:331
160. Stellwagen NC, Gelfi C, Righetti PG (1997) Biopolymers 42:687
161. Olivera BM, Baine P, Davidson N (1964) Biopolymers 2:245
162. Fawcett JS, Morris CJOR (1966) Separ Sci 1:9
163. Ogston AG (1958) Trans Faraday Soc 54:1754
164. Rodbard D, Chrambach A (1970) Proc Natl Acad Sci USA 65:970
165. Chrambac A, Rodbard D (1971) Science 172:440
166. Ferguson KA (1964) Metabolism 13:985
167. Stellwagen NC, Stellwagen E (2009) J Chromatogr A 1216:1917
168. Chiari M, Cretich M, Consonni R (2002) Electrophoresis 23:536
169. Barbier V, Buchholz BA, Barron AE, Viovy J-L (2002) Electrophoresis 23:1441
170. Madabhushi RS, Vainer M, Dolnik V, Enad S, Barker DL, Harris DW, Mansfield ES (1997) Electrophoresis 18:104
171. Chiari M, Riva S, Gelain A, Vitale A, Turati E (1997) J Chromatogr A 781:347
172. Heller C (1999) Electrophoresis 20:1962
173. Xu F, Baba Y (2004) Electrophoresis 25:2332
174. Sunada WM, Blanch HW (1997) Electrophoresis 18:2243
175. Cottet H, Gareil P (2002) Electrophoresis 23:2788
176. Albarghouthi MN, Buchholz BA, Doherty EAS, Bogdan FM, Zhou H, Barron AE (2001) Electrophoresis 22:737
177. Buchholz BA, Barron AE (2001) Electrophoresis 22:4118
178. Njoroge SK, Witek MA, Hupert ML, Soper SA (2010) Electrophoresis 31:981
179. Doherty EAS, Kan CW, Barron AE (2003) Electrophoresis 24:4170
180. Doherty EAS, Kan CW, Paegel BM, Yeung SHI, Cao ST, Mathies RA, Barron AE (2004) Anal Chem 76:5249
181. Ekani-Nkodo A, Tinland B (2003) Phys Rev E 67:051920
182. Shi X, Hammond RW, Morris MD (1995) Anal Chem 67:1132
183. Viovy J-L, Duke T (1993) Electrophoresis 14:322
184. Klein J (1978) Macromolecules 11:852
185. Mayer P, Slater GW, Drouin G (1994) Anal Chem 66:1777
186. Netter H (1969) Theoretical biochemistry. Wiley, New York, 87
187. Heller C, Slater GW, Mayer P, Dovichi N, Pinto D, Viovy JL, Drouin G (1998) J Chromatogr A 806:113
188. Desruisseaux C, Drouin G, Slater GW (2001) Macromolecules 34:5280
189. Desruisseaux C, Slater GW, Drouin G (1998) Macromolecules 31:6499
190. Ulanovsky L, Drouin G, Gilbert W (1990) Nature 343:190
191. Ren H, Karger AE, Oaks F, Menchen S, Slater GW, Drouin G (1999) Electrophoresis 20:2501
192. Vreeland WN, Meagher RJ, Barron AE (2002) Anal Chem 74:4328
193. Sinville R, Coyne J, Meagher RJ, Cheng Y-W, Barany F, Barron A, Soper SA (2008) Electrophoresis 29:4751

194. Fodor SPA, Read JL, Pirrung MC, Stryer L, Lu AT, Solas D (1991) Science 251:767
195. Fodor SPA, Rava RP, Huang XHC, Pease AC, Holmes CP, Adams CL (1993) Nature 364:555
196. Schena M, Shalon D, Davis RW, Brown PO (1995) Science 270:467
197. Churchill GA (2002) Nat Genet 32:490
198. Heller MJ (2002) Annu Rev Biomed Eng 4:129
199. Venkatasubbarao S (2004) Trends Biotechnol 22:630
200. Syvanen AC (2005) Nat Genet 37:S5
201. Hoheisel JD (2006) Nat Rev Genet 7:200
202. Guo Z, Guilfoyle RA, Thiel AJ, Wang RF, Smith LM (1994) Nucleic Acids Res 22:5456
203. Joos B, Kuster H, Cone R (1997) Anal Biochem 247:96
204. Erickson D, Liu XZ, Krull U, Li DQ (2004) Anal Chem 76:7269
205. Yuen PK, Li GS, Bao YJ, Muller UR (2003) Lab Chip 3:46
206. Lenigk R, Liu RH, Athavale M, Chen ZJ, Ganser D, Yang JN, Rauch C, Liu YJ, Chan B, Yu HN, Ray M, Marrero R, Grodzinski P (2002) Anal Biochem 311:40
207. Wang Y, Vaidya B, Farquar HD, Stryjewski W, Hammer RP, McCarley RL, Soper SA, Cheng YW, Barany F (2003) Anal Chem 75:1130
208. Hashimoto M, Barany F, Soper SA (2006) Biosens Bioelectron 21:1915
209. Xu F, Datta P, Wang H, Gurung S, Hashimoto M, Wei S, Goettert J, McCarley RL, Soper SA (2007) Anal Chem 79:9007
210. Hupert ML, Wang H, Chen H-W, Chen PC, Stryjewski W, Patterson D, Witek MA, Datta P, Goettert J, Murphy MC, Soper SA (2008) A field-deployable system for automated molecular testing using modular microfluidics. In: 12th international conference on miniaturized systems for chemistry and life sciences, μTAS2008, 12-16 October 2008, San Diego, California, USA, pp 1946
211. Situma C, Wang Y, Hupert M, Barany F, McCarley RL, Soper SA (2005) Anal Biochem 340:123
212. Rasmussen SR, Larsen MR, Rasmussen SE (1991) Anal Biochem 198:138
213. Csaki A, Moller R, Straube W, Kohler JM, Fritzsche W (2001) Nucleic Acids Res 29:E81
214. Ahn S, Walt DR (2005) Anal Chem 77:5041
215. Fan ZH, Mangru S, Granzow R, Heaney P, Ho W, Dong QP, Kumar R (1999) Anal Chem 71:4851
216. Ali MF, Kirby R, Goodey AP, Rodriguez MD, Ellington AD, Neikirk DP, McDevitt JT (2003) Anal Chem 75:4732
217. Schena M, Shalon D, Heller R, Chai A, Brown PO, Davis RW (1996) Proc Natl Acad Sci USA 93:10614
218. Cheung VG, Morley M, Aguilar F, Massimi A, Kucherlapati R, Childs G (1999) Nat Genet 21:15
219. McCarley RL, Vaidya B, Wei SY, Smith AF, Patel AB, Feng J, Murphy MC, Soper SA (2005) J Am Chem Soc 127:842
220. Wei SY, Vaidya B, Patel AB, Soper SA, McCarley RL (2005) J Phys Chem B 109:16988
221. Liu YJ, Rauch CB (2003) Anal Biochem 317:76
222. Wei CW, Cheng JY, Huang CT, Yen MH, Young TH (2005) Nucleic Acids Res 33:e78
223. Yaralioglu GG, Wygant IO, Marentis TC, Khuri-Yakub BT (2004) Anal Chem 76:3694
224. Vanderhoeven J, Pappaert K, Dutta B, Vanhummelen P, Baron GV, Desmet G (2004) Electrophoresis 25:3677
225. Sternberg JC (1966) Adv Chromatogr 2:205
226. Harvey MC, Stearns SD (1983) J Chromatogr Sci 21:473
227. Claemsens HA, Burcinova A, Cramers CA, Mussche P, van Tilburg CCE (1990) J Microcolumn Sep 2:132
228. Blas M, Delaunay N, Rocca J-L (2008) Electrophoresis 29:20
229. Fan ZH, Harrison DJ (1994) Anal Chem 66:177
230. Harrison DJ, Fan ZH, Seiler K, Manz A, Widmer HM (1993) Anal Chim Acta 283:361

231. Effenhauser CS, Manz A, Widmer HM (1993) Anal Chem 65:2637
232. Effenhauser CS, Paulus A, Manz A, Widmer HM (1994) Anal Chem 66:2949
233. Wenclawiak BW, Puschl R (2006) Anal Lett 39:3
234. Figeys D, Ahmadzedeh H, Arriaga E, Dovichi NJ (1996) J Chromatogr A 744:325
235. Lin CC, Chen CC, Lin CE, Chen SH (2004) J Chromatogr A 1051:69
236. Kim DK, Kang SH (2005) J Chromatogr A 1064:121
237. Jacobson SC, Koutny LB, Hergenroder R, Moore AW, Ramsey JM (1994) Anal Chem 66:3472
238. Chien RL, Burgi DS (1991) J Chromatogr 559:141
239. Bharadwaj R, Santiago JG, Mohammadi B (2002) Electrophoresis 23:2729
240. Khandurina J, Jacobson SC, Waters LC, Foote RS, Ramsey JM (1999) Anal Chem 71:1815
241. Kelly RT, Li Y, Woolley AT (2006) Anal Chem 78:2565
242. Strausbauch MA, Landers JP, Wettstein PJ (1996) Anal Chem 68:306
243. Pedersen-Bjergaard S, Rasmussen KE, Halvorsen TG (2000) J Chromatogr A 902:91
244. Muscate A, Natt F, Paulus A, Ehrat M (1998) Anal Chem 70:1419
245. Burns MA, Johnson BN, Brahmasandra SN, Handique K, Webster JR, Krishnan M, Sammarco TS, Man PM, Jones D, Heldsinger D, Mastrangelo CH, Burke DT (1998) Science 282:484
246. Walker GT, Fraiser MS, Schram JL, Little MC, Nadeau JG, Malinowski DP (1992) Nucleic Acids Res 20:1691
247. Hashimoto M, Barany F, Xu F, Soper SA (2007) Analyst 132:913
248. Simpson PC, Woolley AT, Mathies RA (1998) Biomed Microdevices 1:7
249. Belgrader P, Smith JK, Weedn VW, Northrup MA (1998) J Forensic Sci 43:315
250. Northrup MA, Benett B, Hadley D, Landre P, Lehew S, Richards J, Stratton P (1998) Anal Chem 70:918
251. Zhang N, Tan H, Yeung ES (1999) Anal Chem 71:1138
252. Thaitrong N, Toriello NM, Del Bueno N, Mathies RA (2009) Anal Chem 81:1371
253. Olsen KG, Ross DJ, Tarlov MJ (2002) Anal Chem 74:1436
254. Toriello NM, Douglas ES, Thaitrong N, Hsiao SC, Francis MB, Bertozzi CR, Mathies RA (2008) Proc Natl Acad Sci USA 105:20173
255. Toriello NM, Liu CN, Blazej RG, Thaitrong N, Mathies RA (2007) Anal Chem 79:8549
256. Budowle B, van Daal A (2009) Biotechniques 46:339
257. Grover WH, Skelley AM, Liu CN, Lagally ET, Mathies RA (2003) Sens Actuators B 89:315
258. Liu P, Yeung SHI, Crenshaw KA, Crouse CA, Scherer JR, Mathies RA (2008) Forensic Sci Int Genet 2:301
259. Ewing B, Hillier L, Wendl MC, Green P (1998) Genome Res 8:175
260. Yeung SW, Lee TMH, Cai H, Hsing IM (2006) Nucleic Acids Res 34:e118
261. Yeung SSW, Lee TMH, Hsing IM (2008) Anal Chem 80:363
262. Liu RH, Yang JN, Lenigk R, Bonanno J, Grodzinski P (2004) Anal Chem 76:1824